

Floquet breathers in a modulated nonlinear lattice

Masayuki Kimura,¹ Juan F. R. Archilla,^{2, a)} Yusuke Doi,³ and Víctor J. Sánchez-Morcillo⁴

¹⁾Department of Electrical and Electronic Engineering, Faculty of Science and Engineering
Setsunan University, 17-8 Ikeda-Nakamachi, Neyagawa, Osaka 572-8508, Japan

²⁾Grupo de Física No Lineal, Universidad de Sevilla, ETSI Informática, Avda Reina Mercedes s/n, 41012-Sevilla, Spain

³⁾Division of Mechanical Engineering, Graduate School of Engineering, The University of Osaka, 2-1 Yamadaoka, Suite, Osaka 565-0871, Japan

⁴⁾Universitat Politècnica de València, Instituto de Investigación para la Gestión Integrada de Zonas Costeras (IGIC), Paranimf 1, 46730 Grao de Gandia, València, Spain

In this work, we study a space-time modulated electro-mechanical system, consisting of an array of coupled cantilevers with their on-site potential provided by electromagnets driven by AC currents. Model equations are derived, and the effect of the modulation on the dispersion bands is examined. The theory of breather existence and stability is extended to include space-time modulation. We perform numerical simulations in a time-modulated system, showing three types of breather response depending on the driving frequency: (i) the modulation frequency is an integer multiple of the breather frequency or, in other words, this phenomenon corresponds to period doubling, tripling, etc.; (ii) the opposite, that is, the breather frequency is an integer multiple of the modulation frequency, corresponding to period-halving, etc. (iii) the breather and modulation frequencies are commensurate in a different form. We use for all of them the term *Floquet breathers* in analogy with Floquet solitons in photonic systems. As there is no dissipation, but periodic forcing, the energy is conserved but only at discrete times. There exists in this system a huge variety of breathers, either site-centered, symmetric and antisymmetric, bond centered, in-phase or in-quadrature with the modulation, and we analyze the evolution of stability of some of them as a function of the modulation frequency. The construction of a similar system would be of interest to study the properties of dynamic metamaterials.

PACS numbers: 63.20.Pw, 63.20.Ry, 05.45.-a, 02.70.-c

Keywords: nonlinear waves, breathers, thermal equilibrium, localization, intrinsic localized modes (ILM)

I. INTRODUCTION

Highly localized periodic vibrations, so-called intrinsically localized modes (ILM) or discrete breathers (DB), are ubiquitous in many nonlinear lattice-type systems. First reported in ¹, ILMs have been shown to exist with different spatial patterns; the simplest one is the Sievers-Takeno (ST) mode, where a single oscillator, called the center, has an amplitude much larger than its nearest neighbors, so the amplitude decreases rapidly with the distance to the center. Other mode is the Page (P) mode ^{2,3}, where two neighboring oscillators have the same amplitude, either in-phase or anti-phase, being therefore a double ILM or breather.

An important issue regarding ILMs concerns their stability. In Fermi-Pasta-Ulam-Tsingou (FPUT) lattices with an anharmonic interaction, ST modes are unstable, while P modes are often stable. The stability of these modes is related to their spatial symmetry and the Peierls-Nabarro potential barrier³. In contrast, the stability properties of these modes depend on the class of lattice model considered. In lattices with nonlinear on-site potentials, such as nonlinear Klein-Gordon (NKG) systems, rigorous results based on the anti-continuum limit show that ST modes exist and are linearly stable under appropriate non-resonance conditions, irrespective of

whether the on-site potential is soft or hard, where softness (hardness) corresponds to a decrease (increase) of the oscillation frequency with increasing amplitude. The stability of P modes in such systems is more subtle and may involve stability exchange with ST modes as system parameters are varied ⁴.

The study of breather stability were considerably enhanced by Aubry's band theory, where the eigenvalues of the Newton operator, that is, the operator corresponding to the perturbation of a breather, allow for precise determination of the stability and structural stability of breathers and multibreathers ⁵.

In this work, we are interested in breathers in a time-periodic nonlinear system. We will use the term *Floquet breathers*, similar to Floquet solitons used in photonic systems ^{6–10}. Therefore, Floquet breathers are time-periodic, spatially localized vibrations in discrete, time-periodic nonlinear systems. The breather period does not need to be the period of the system, but commensurate with it as used in the last references. We will consider a specific time-periodic nonlinear system as described below.

Arrays of coupled cantilevers have played a relevant role in the study of nonlinear vibrations, in particular on energy localization¹¹, and are among the physical systems where breathers have been reported. They can be built at very different sizes, including nano-, micro- and macro-scales, and can be driven by different types of forces. They are part of important applications, such

^{a)}Corresponding author: archilla@us.es

as actuators and sensors. An experimental macroscopic array of cantilevers was presented in Ref. ¹². The system was driven by a periodic force applied to the support of the cantilevers, appearing as an independent external (additive) force in the dynamical equations. The restoring force had two contributions: one provided by the elastic properties of the cantilever, and other of magnetic nature, by fixing a magnet at the free end of the cantilever, and locating an electromagnet below it. The magnetic force due to permanent magnet-electromagnet interaction, can be tuned by changing an electric DC current, in this way, a tunable on-site potential is obtained.

The system resulted in breathers having different properties depending on the current magnitude and the frequency. These and similar models have been used in the study of ILMs ¹³⁻¹⁷.

In this paper we present a variation of the model introduced in Ref. ¹², but incorporating, besides the static (DC) current, an oscillating (AC) contribution in the electromagnets. This brings about an on-site potential that it is tunable and periodic in time. Furthermore, introducing phase differences between neighboring cantilevers, an on-site potential with a space-time modulation is achieved. An experimental and mathematical model with a linear on-site potential and nonlinear coupling has been studied ¹⁸, finding q -gap breathers. In our case the on-site potential is nonlinear and the coupling is linear.

The article is organized as follows: after the introduction in Sec. I, Sec. II presents the physical model and the derivation of the system of differential equations, both for the nonlinear system and its linear approximation corresponding to small oscillations. In Sec. III, the effect of space and time modulation on the dispersion bands is presented, while the theoretical deduction is located in Appendix B. Sec. IV presents changes brought about by modulation in breather theory, breather obtention, and stability. Sec. V, presents breathers with a period that is an integer of the modulation period, and thus with a frequency smaller than the modulating one, and their properties are analyzed. The case of the breather frequency as a multiple of the modulating frequency is presented in Sec. VI. Sect. VII considers also rational ratios of the breather and modulation frequencies and the possibility of the breathers to be in quadrature with the modulation. A systematic study of the evolution of stability with the frequency is performed. The final Sec. VIII presents the concluding remarks. As already stated, the mathematical deduction of the dispersion relations is included in Appendix B, preceded by Appendix A introducing the notation used and some concepts perhaps not familiar to some readers.

II. PHYSICAL SYSTEM AND DYNAMICAL EQUATIONS

In this section we derive from physical laws the dynamical equations. A sketch of the physical model is shown in Fig. 1.

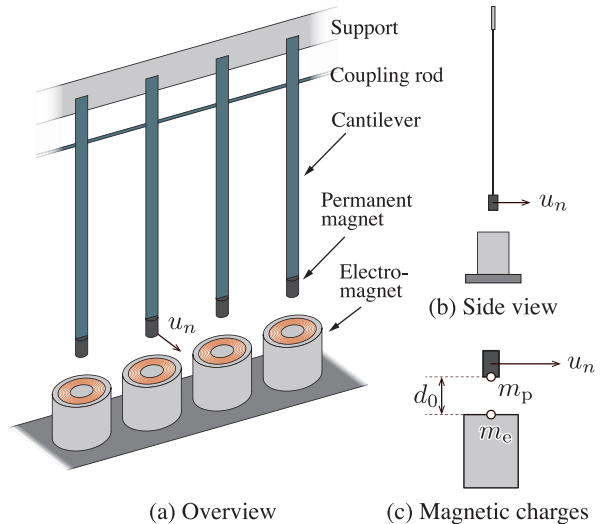


FIG. 1. System of cantilevers mechanically coupled by a rod. (b) Side view of a cantilever. A permanent magnet is attached to the tip of the cantilever. An electromagnet is placed below the permanent magnet. (c) Definition of magnetic charges. Modified with permission from Ref. ¹²

The variable u_n measures the horizontal deviation of the cantilever tip with respect to its equilibrium position. The vertical distance between the electromagnet and the cantilever tip is y_n , therefore, the position vector of the tip with respect to the electromagnet is $\vec{r}_n = u_n \hat{e}_x + y_n \hat{e}_y$, with equilibrium position $\vec{r}_{n,0} = d_0 \hat{e}_y$, and modulus $r_n = \sqrt{u_n^2 + y_n^2}$. Within the formulation of magnetic charges, analogous to the Coulomb law, the magnetic force is given by $\vec{F}(\vec{r}_n) = \frac{1}{4\pi\mu_0} \frac{m_p m_e}{r_n^2} \hat{r}_n$ ¹⁹ with m_p and m_e the magnetic charges of the permanent magnet and the electromagnet, respectively, and \hat{r}_n the unitary vector in the direction of \vec{r}_n . Assuming small cantilever angles, $y_n \simeq d_0$ and the horizontal force component per unit mass becomes

$$F(u_n) = \frac{m_p m_e}{4\pi\mu_0 M} \frac{u_n}{(u_n^2 + d_0^2)^{3/2}}. \quad (1)$$

The strength of the magnetic force is controlled by the current I_{EM} of the electromagnet. The first factor in Eq.(1) can be identified with an interaction coefficient (force per unit mass), $\chi(I_{EM})$, which may be alternatively expressed as a function of the driving current I_{EM} as $\chi(I_{EM}) = \chi_0 + \chi_1 I_{EM}$. The constant term χ_0 in the interaction coefficient is due to the ferromagnetic core of the electromagnet, while the variable term χ_1 is due to

the magnetic field created by the current of the electromagnet. Note that $\chi_0 < 0$, corresponding to an attractive force, and χ_1 depends on the polarity of the current, which is such that in this work $\chi_1 < 0$ too. The current consists of a DC and a modulated AC components, i.e.,

$$I_{EM}(n, t) = I_{DC} + I_{AC} \cos(hn - \Omega t) \quad (2)$$

Therefore the dynamical equations become:

$$\ddot{u}_n = -\omega_{0,0}^2 u_n + F(u_n) + C(u_{n+1} + u_{n-1} - 2u_n) \quad (3)$$

where $\omega_{0,0}$ is the natural frequency of an isolated cantilever (which, according to Euler–Bernoulli beam theory, depends on his geometry and the material properties), C is a coupling constant, and the force is given by

$$F(u_n) = -(|\chi_0| + |\chi_1| I_{EM}(n, t)) \frac{u_n}{(u_n^2 + d_0^2)^{3/2}} \quad (4)$$

Typical values of the parameters for the cantilever system, obtained in a previous experiment, are $\omega_{0,0} = 2\pi \times 35.72 \text{ rad/s}$, $d_0 = 3 \text{ mm}$, $\chi_0 = -4.71 \times 10^{-5} \text{ m}^3 \text{s}^{-2}$, $\chi_1 = -9.14 \times 10^{-3} \text{ m}^3 \text{s}^{-2} \text{ A}^{-1}$ and $C = 284 \text{ s}^{-2}$.

Expanding the last term in Eq.(4), results in

$$\frac{u_n}{(u_n^2 + d_0^2)^{3/2}} = \frac{u_n}{d_0^3} - \frac{3}{2} \frac{u_n^3}{d_0^5} + o(u_n^5) \quad (5)$$

evidencing that the on-site potential is of soft type. Keeping only the linear term, we obtain the linearized equations:

$$\begin{aligned} \ddot{u}_n = & -\omega_{0,0}^2 u_n \\ & - \left(\frac{|\chi_0| + |\chi_1| I_{DC}}{d_0^3} + \frac{|\chi_1| I_{AC}}{d_0^3} \cos(hn - \Omega t) \right) u_n \\ & + C(u_{n+1} + u_{n-1} - 2u_n), \end{aligned} \quad (6)$$

The frequency of small oscillations of an isolated oscillator, in the absence of modulation, is $\omega_{0,\text{phys}} = (\omega_{0,0}^2 + \frac{|\chi_0| + |\chi_1| I_{DC}}{d_0^3})^{1/2}$. We can re-scale the magnitudes in a relatively complicated way to obtain simpler equations, by using $\tau = 1/\omega_{0,\text{phys}}$ and σ such as $\sigma^3 = \frac{|\chi_0| + |\chi_1| I_{DC}}{\omega_{0,\text{phys}}^2}$, as units of time and distance, respectively. The scaled linear equations become

$$\ddot{u}_n = -\omega_0^2 u_n - \delta \cos(hn - \Omega t) u_n + \kappa(u_{n+1} + u_{n-1} - 2u_n), \quad (7)$$

with $\omega_0 = 1$, that we keep for clarity, $\kappa = C/\omega_{0,\text{phys}}^2$, and $\delta = \frac{|\chi_1| I_{AC}}{\omega_{0,\text{phys}}^2 d_0^3}$.

The non-linearized model, in the scaled variables, results

$$\begin{aligned} \ddot{u}_n = & -\omega_0^2 u_n \\ & - \omega_0^2 \left(-\frac{1}{d_0^3} u_n + (1 + \delta \bar{d}_0^3 \cos(hn - \Omega t)) \frac{u_n}{(u_n^2 + \bar{d}_0^2)^{3/2}} \right) \\ & + \kappa(u_{n+1} + u_{n-1} - 2u_n), \end{aligned} \quad (8)$$

for $\bar{d}_0 = d_0/\sigma$. The second term multiplied by $\omega_0^2 = 1$ is written in that way because it is completely nonlinear when expanding the terms in u_n . It also highlights that the linear frequency of the unmodulated system of the isolated oscillator is $\omega_0 = 1$.

The nonlinear equations in a more condensed form are:

$$\begin{aligned} \ddot{u}_n = & -\omega_0^2 u_n \\ & - \omega_0^2 \left(-\delta_1 u_n + (1 + \delta_2 \cos(hn - \Omega t)) \frac{u_n}{(u_n^2 + \bar{d}_0^2)^{3/2}} \right) \\ & + \kappa(u_{n+1} + u_{n-1} - 2u_n), \end{aligned} \quad (9)$$

with $\delta_1 = 1/\bar{d}_0^3$ and $\delta_2 = \delta \bar{d}_0^3$.

For a representative set of parameters of currents, we fix DC and AC amplitudes as $I_{AC} = I_{DC} = 12 \text{ mA}$, and in order to obtain that $\omega_0 = 1$, the scaling factors are $\tau = 4.286 \text{ ms}$ and $\sigma = 1.423 \text{ mm}$, leading to $\bar{d}_0 = 2.1087$, $\kappa = 0.0051632$, $\delta_1 = 0.10665$, $\delta_2 = 0.6996$.

The linearization of (9) leads again to the system (7), with $\delta = \delta_2/\bar{d}_0^3 = \delta_2 \delta_1 = 0.07461$ for the chosen currents.

In the following we will write d_0 instead of \bar{d}_0 for simplicity.

III. EFFECT OF SPACE-TIME MODULATION ON THE PHONON DISPERSION RELATION

In this section, we present the main consequences of space-time modulation of the linear system (7). They are also valid for small displacements $u_n(t)$ in the non-linearized model (9). The relatively detailed mathematical derivations based on Bloch theorem is included in Appendix B.

For $\delta = 0$, that is, without modulation, the phonon dispersion relation (PDR) is given by $\omega_q^2 = \omega_0^2 + 2\kappa(1 - \cos(q))$ as a function of the wave number q of the phonon. In this work, the minimum frequency $\omega_0 = 1$ and the maximum one $\sqrt{\omega_0^2 + 4\kappa} = 1.01$ for $\kappa = 0.052$. Numerically, the phonon spectrum can be obtained using the two-dimensional fast Fourier transform of $u_n(t)$ in space and time (XTFFT) as explained in App. B.1.

For modulation frequencies Ω that are a few times smaller than ω_0 , the main effect is the emergence of several replicas of the phonon dispersion curves, whose maxima are shifted and vertically displaced (in frequency) relative to the unmodulated dispersion curves, as shown in the bottom panel of Fig. 2. The energy density plot for the same simulation is also presented in the upper panel of Fig. 2.

In App. B.3 it is deduced that to first order approximation the effect of time modulation alone is given by

$$\omega = -m\Omega + \sqrt{\omega_0^2 + 2\kappa(1 - \cos(q))}, \quad (10)$$

with $m = \pm 1, \pm 2, \pm 3, \dots$.

Figure 3 presents two plots of the PDR obtained numerically for two different values of Ω .

If there are both time and space modulation it is also deduced in App. B.4 that the phonon bands are given by:

$$\omega = -m\Omega + \sqrt{\omega_0^2 + 2\kappa(1 - \cos(q + mh))}. \quad (11)$$

Figure 4 represents both the theoretical and numerically obtained PDR, showing a very good agreement.

The derivations presented in Appendix B cannot predict the intensity of the various PDR. In App. B.2, it is also deduced the effect of symmetry breaking of the space invariance by only space modulation.

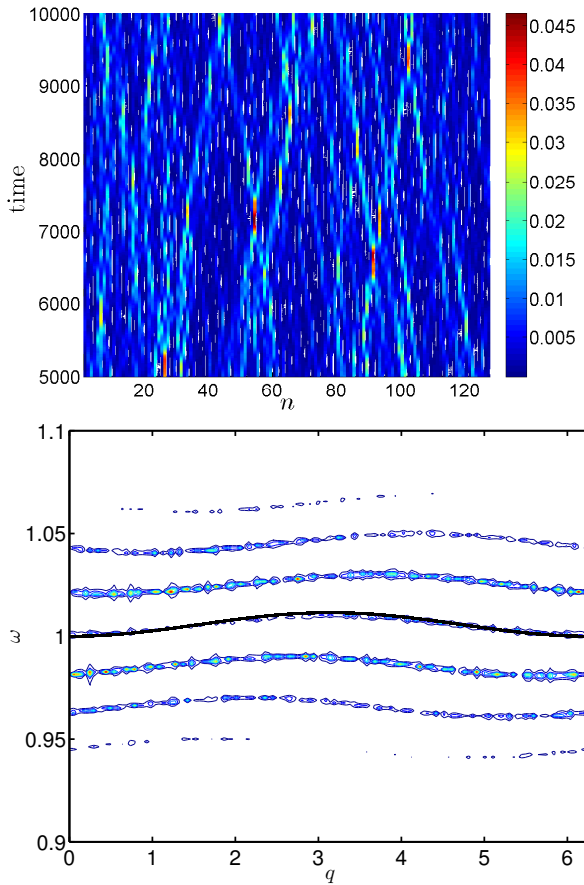


FIG. 2. Numerical simulations after thermalization of the linear system. See App. B.1 for details. (**Top:**) Energy density plot (**Bottom**) Contour plot of the two-dimensional XFFT of the coordinates $u_n(t) = u(n, t)$ as a function of n and t . Parameters: $\kappa = 0.0052$, $\delta = 0.075$, $\Omega = 0.02$, $h = 0.5$, $N = 128$.

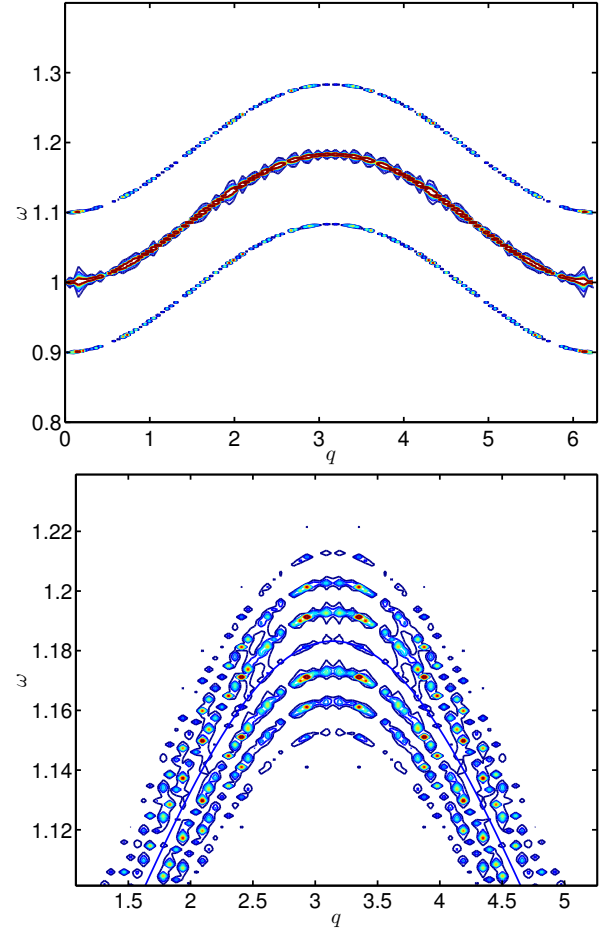


FIG. 3. Contour plot of the XFFT after thermalization of the linear system with only time modulation. See App. B.1 for details. Parameters: $\kappa = 0.1$, $\delta = 0.075$, $h = 0$, $N = 120$ (Top panel) $\Omega = 0.1$; (Bottom panel) $\Omega = 0.01$

IV. BREATHERS WITH SPACE-TIME MODULATION

In this section we study the conditions for breather existence in a modulated system, first reviewing the theory of exact breathers and adapting it to space-time modulation and to just time modulation.

IV.A. Exact traveling breathers

The theory of moving breathers was developed by Aubry and coauthors in Refs.^{20,21} and Flach²² among others. We will refer here to a formulation very similar to the latter, developed by some of the authors to interpret exact moving breathers in the $q - \omega$ space²³. Other articles related to that formulation are Ref.²⁴ with a rigorous mathematical treatment, and²⁵ applied to the DNLS, where the concept of resonant lines (see below) appear. Here, we adapt the formulation in Ref.²³ to modulated systems.

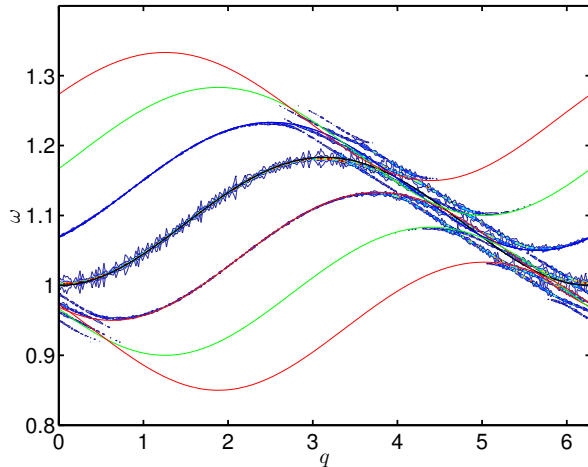


FIG. 4. Contour plot of the XTFFT after thermalization of the linear system with both time and space modulation, together with the theoretical dispersion curves. See App. B.1 and B.4 for details. Parameters: $\delta = 0.05$, $\Omega = 0.05$, $\kappa = 0.1$, $h = 0.5$, $N=120$. Note that there is an area to the right where the harmonics are very close and become mixed.

Let us suppose that we have a space-time modulated system with phase $\phi = hn - \Omega t$ and velocity $V_m = h/\Omega$. An exact breather will be a solution of the form²²:

$$u(n, t) = f(n - V_b t, \omega_i t), \quad (12)$$

where the function f is a localized function of its first argument and a 2π periodic function of the second, and V_b is the velocity of the breather. If the breather is exact, there exists a minimal time T_F , called the fundamental time, and an integer s , called the step, such after a time T_F , the breather reproduces itself displaced a distance s in lattice units. Then, $V_b = s/T_F$, and the fundamental frequency is defined as $\omega_F = 2\pi/T_F$. The frequency ω_i , is the moving frame frequency²³ also called internal frequency²².

The condition for $u(n, t)$ to be exact is that $u(n + s, t + T_F) = u(n, t)$, which implies that $s = V_b T_F$ and $\omega_i = m\omega_F$. Harmonic functions with the same symmetry (same step and fundamental frequency) are called resonant harmonics and form a basis for the breather. They can be written as

$$\exp(i(q[n - V_b t]) \exp(-im\omega_F t) = \exp(i[qn - \omega_L t]) \\ \text{with } \omega_L = qV_b + m\omega_F. \quad (13)$$

where ω_L and $m\omega_F$ are the laboratory and moving frame frequencies, respectively, of the resonant harmonic.

The resonant harmonics form straight lines within the (q, ω) space, called *resonant lines*. Their slope is V_b and their intercept at the axis $q = 0$ is $m\omega$, i.e, the moving frame frequency. Therefore, all the harmonics in a resonant line have the same frequency $m\omega_F$, with the integer m indexing the lines.

The breather frequencies are inside one of those lines called the *breather line* with $m = m_b$. The intercept of the breather line with the axis $q = 0$ is the moving frame frequency of the breather $\omega_b = m_b\omega_F$. All the harmonic waves in the same line have the same frequency in the moving frame and propagates with the same velocity V_b , which explains the persistence of the breather.

For a soft potential as in our case, the breather line will be below the phonon band, and close to its minimum at $q = 0$. If the breather line intersects the phonon band, the intersection phonon will be excited leading to a wing, an extended quasi-linear harmonic wave attached to the breather, with amplitude depending on the specific system and the frequency, and sometimes being zero.

IV.B. Application to space-time harmonically modulated systems

For a space-time harmonically modulated system with a term $\cos(hn - \Omega t)$, it is also necessary that the value of the modulating phase $\Phi = hn - \Omega t$ is also identical modulo 2π after the translation s and time change T_F , because if not, the forces will be different and the evolution of u would be different.

Therefore:

$$h(n + s) - \Omega(t + T_F) = hn - \Omega t + 2\pi m_m \rightarrow \\ \Omega = \frac{hs + 2\pi r}{T_F} \rightarrow \Omega = hV_b + m_m\omega_F. \quad (14)$$

This means that the modulating wave is a resonant harmonic with index m_m and moving frame frequency $m_m\omega_F$ and therefore the breather and modulating waves have commensurate moving frame frequencies.

Lemma 1 *A necessary condition for an exact breather within a space-time modulated system with harmonic modulation is that the modulating harmonic is within a resonant line with the breather, or, in other words, that their moving frame frequencies are both integer multiples of the fundamental frequency ω_F . Therefore ω_b and Ω are commensurate.*

The immediate consequence for only time modulation is:

Lemma 2 *For a harmonically, time-modulated system, a necessary condition for breather existence is that the breather frequency ω_b and the modulating frequency Ω are commensurate: $\omega_b/\Omega = m_b/m_m$.*

IV.C. Breather obtention in the time-modulated system

The most direct way is working in the real space with the Newton and shooting method. Trying some different localized initial conditions and observing an approximate periodical behavior with period close to T_b , the intended one, the initial conditions are used as a seed for the Newton method, where initial conditions corresponding to the exact T_b -periodic behavior. Exact means with

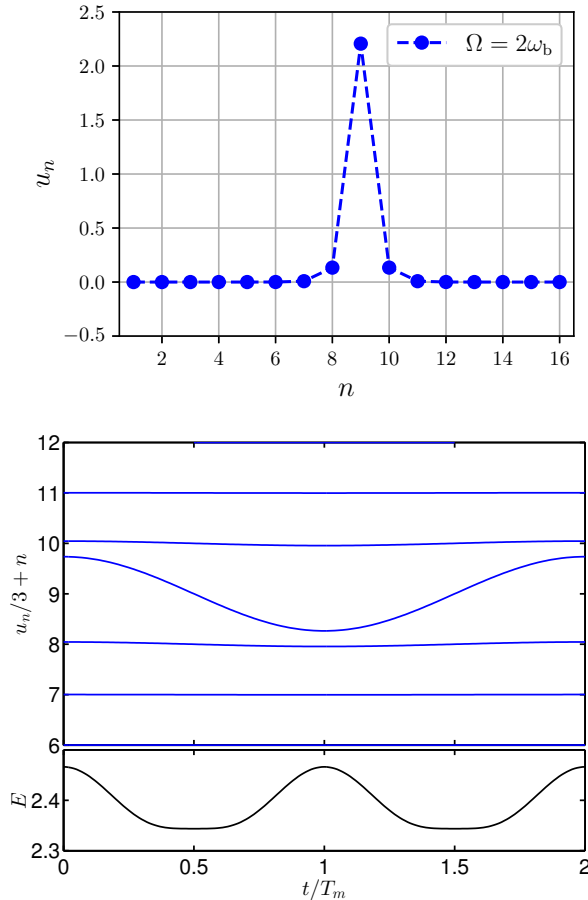


FIG. 5. (Top) For $\Omega = 2\omega_b$, profile of the stable breather. (Bottom) Coordinates and energy evolution in a breather period T_b . Parameters: $\kappa = 0.0052$, $\delta_1 = 0.1067$, $\delta_2 = 0.6996$, $\omega_b = 0.98$.

a precision of 10^{-15} , that is, very close, to the computer machine precision. The Newton method, a numerical application of the implicit function theorem, can be used as the system has no time invariance due to the time-periodic term in the potential, and a solution is unique in its neighborhood. The precision can be refined more by working in the space of the frequencies, if we consider time-reversible solutions, they can be written as $u_n(t) = \sum_{k=-k_m}^{k_m} z_{k,n} \exp(k\omega_b t)$. Due to $u_n(t)$ being real and time-symmetric, $z_{k,n}^* = z_{-k,n}$ and $z_{k,n} = z_{-k,n}$, and real. The $u_n(t) = z_{0,n} + \sum_{k=1}^{k_m} 2z_{k,n} \cos(k\omega_b t)$, being $2z_{k,n}$ the inverse cosine fast Fourier cosine transform (idfc). Then, the Newton method can be coded in the space of the $k_m + 1$ FFT components, finding the fftc components $z_{n,k}$. The value of $m = 15$ provides excellent results.

The breather initial coordinates for the case $\Omega = 2\omega_b$ are represented in Fig. 5-top, the initial velocities being zero.

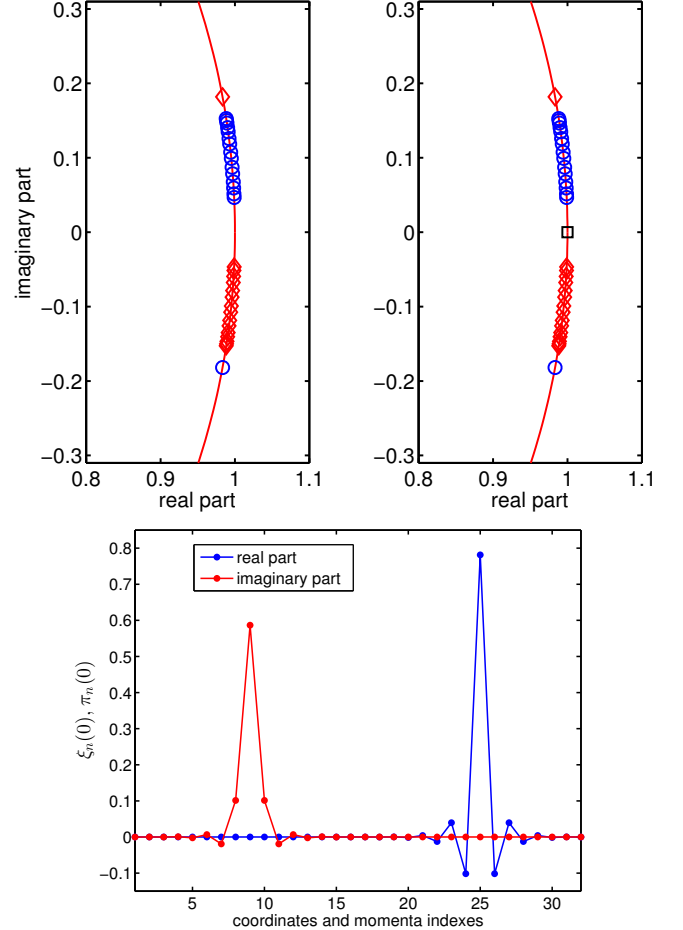


FIG. 6. For $\Omega = 2\omega_b$: (Top-left) Floquet multipliers for the non-autonomous system and (top-right) for the extended autonomous system. Blue circles have positive Krein signature, red diamonds negative one, and black squares correspond to zero Krein signature. The multipliers are identical except for the double +1 of the extended system. (Bottom panel) Eigenvector corresponding to the isolated eigenvalue, related with localized perturbations of the breather. Parameters: $\kappa = 0.0052$, $\delta_1 = 0.1067$, $\delta_2 = 0.6996$, $\omega_b = 0.98$.

IV.D. Stability of breathers in the time-modulated system

Let us suppose that the breather solution for a breather with $T_b = n_T T_m$, with n_T an integer larger than 1, the T_m -periodic system is also T_b periodic, and to analyze the stability we can construct the Floquet matrix integrating a small perturbation of the initial coordinates and momenta and observing the perturbation after $T = T_b$. For each changed coordinate we obtain a column of the Floquet matrix F . Its eigenvalues lie on the unit circle if the system is stable. For autonomous symplectic systems²⁶ there are always two eigenvalues of F at +1, corresponding to $u_t = \dot{u}$, the phase mode, as it represents that if $u(t)$ is a T_b periodic solution, $u(t + dt)$ is also a solution, and the growth mode, indicating that around a solution

there is another one with slightly different amplitude.

Those two eigenvalues do not generally appear for the non-autonomous system, as can be seen in Fig. 6-top-left for $\Omega = 2\omega_b$. The explanation is that if we write the dynamical equations (9) in a condensed form as:

$$\ddot{u}_n - L_n u_n + (1 + \delta_2 \cos(\Omega t)) \frac{\partial V(u_n)}{\partial u_n} = 0, \quad (15)$$

where $L_n u = -\omega_1^2 u_n + \kappa(u_{n+1} + u_{n-1} - 2u_n)$, with $\omega_1^2 = \omega_0^2 - \delta_1 = \omega_0^2 - 1/d_0^3$, being the linear, unmodulated part of the dynamical system, with $V(0) = 0$; and $V(u_n) = 1/d_0 - 1/\sqrt{d_0^2 + u_n^2}$, the local non-modulated on-site potential.

If $u_b(t)$ is a T_b -periodic solution of (15), and $u(t) = u_b(t) + \xi(t)$ a perturbed solution with $\xi(t)$ small, the evolution of ξ is given by the Newton operator with zero eigenvalue, that is:

$$\begin{aligned} N_n \xi &= \ddot{\xi}_n - L_n \xi \\ &+ (1 + \delta_2 \cos(\Omega t)) \frac{\partial^2 V(u_{b,n}(t))}{\partial u_n^2} \xi_n = 0. \end{aligned} \quad (16)$$

For autonomous systems \dot{u}_b is a solution of (16), but not for non-autonomous ones, as the derivative of (15) is given by:

$$\begin{aligned} \ddot{u}_{b,n} - L_n \dot{u}_{b,n} \\ + (1 + \delta_2 \cos(\Omega t)) \frac{\partial^2 V(u_{b,n}(t))}{\partial u_n^2} \dot{u}_{b,n} \\ - \Omega \delta_2 \sin(\Omega t) \frac{\partial V(u_{b,n}(t))}{\partial u_n} = 0, \end{aligned} \quad (17)$$

where the last term does not appear in (16).

However, it can be recovered within an autonomous extended system that includes the non-autonomous one, as shown below. For the different factors n_T , in $\Omega = n_T \omega_b$, we obtain different results that we will present later.

IV.E. Extended autonomous symplectic system

The Hamiltonian structure of the dynamical equations, i.e., $\dot{u}_n = \partial H/\partial p_n$, $\dot{p}_n = -\partial H/\partial u_n$ is kept for the conjugate pairs of variables u_n , p_n , although the system is no longer autonomous. By defining $s = t$ or to be precise as (16) is T_b -periodic, as $s = \text{rem}(t, T_b)$, the remainder of t/T_b , i.e., $\text{rem}(nT_b + t, T_b) = t$ and $\text{rem}(-nT_b - t, T_b) = -t$, both for $n > 0$ and $t > 0$, so as s is T_b periodic. Then $\dot{s} = 1$ as usual, and the system with the extra variable has become autonomous, but not symplectic as s has no conjugate variable yet. The extra variable h to make the system symplectic is obtained by defining a new Hamiltonian $K = H + h$, with h the conjugate momentum of s as $\dot{s} = \partial K/\partial h = 1$ as previously obtained. Then, $\dot{h} = -\partial K/\partial s = -\partial H/\partial s = -\partial H/\partial t = -dH/dt$, or $h = E_0 - H$, with E_0 the initial energy at $t = 0$ ²⁷.

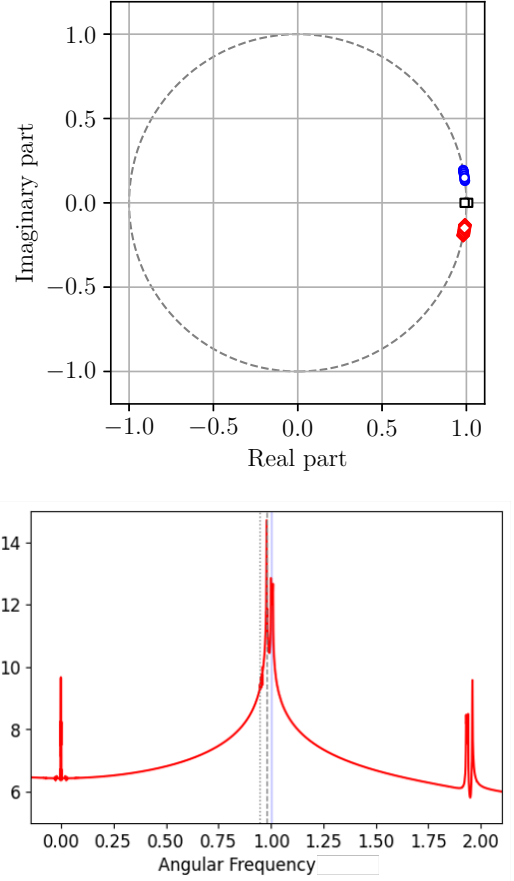


FIG. 7. (Top) Floquet eigenvalues for a breather with $\Omega = 3\omega_b$. (Bottom) Fourier spectra of the same breather embedded in a noisy system with $N = 160$ cantilevers. Parameters: $\kappa = 0.0052$, $\delta_1 = 0.1067$, $\delta_2 = 0.6996$, $\omega_b = 0.98$.

The extended system is now symplectic and $[\dot{u}_b, \dot{s}]$ is now solution of (17) and being T_b periodic, the Floquet multiplier $+1$ corresponding to the *phase mode* reappears. There is an extra $+1$ multiplier, because, symplectiness, implies that the multipliers are in pairs $\lambda, 1/\lambda$, the extra mode corresponding to a solution with slightly different energy or *growth mode*.

The extended system reveals a hidden symplectic structure of the autonomous system with the implication that stability corresponds to all the Floquet multipliers being in the unit circle, but without the double multiplier of $+1$, which is recovered with the extended system. Figure 6-top-right shows these multipliers for $\Omega = 2\omega_b$.

Note these conclusions are valid both the cases $\Omega > \omega_b$ and $\Omega \leq \omega_b$ studied in the next two sections taking due care of the time of integration. They are also valid for space-time modulated systems with trivial changes that we will detail elsewhere.

V. BREathers WITH TIME MODULATION AND

$$\Omega = n_T \omega_b$$

We consider the nonlinear dynamical system (9) with two main cases, $\omega_b = \Omega/n_T$ ($T_b = n_T T_m$), and $\omega_b = n_T \Omega$ ($T_b = T_m/n_T$), n_T an integer. The first one corresponds to the well known phenomenon of period doubling, tripling, etc., while the latter correspond to a breather that oscillates several times faster than the modulation. According to the deduction in Sec. IV, fractional frequencies are also possible and we will consider them in Sec. VII.

There is no dissipation of energy, but as the system is parametrically forced the energy is conserved only at discrete times separated by the larger of the two periods, the breather period T_b and the modulating one T_m . This is shown in Fig. 5 for $T_b = 2T_m$.

In this section we consider $\omega_b = \Omega/n_T$ and leave the condition of $\omega_b > \Omega$ for the next section.

The dynamical equations (9) are invariant under the transformation $t \rightarrow t + T_m$, therefore, if a phonon (q, ω) , i.e., $u = \exp(i[qn - \omega t])$ is a solution of the linearized equation, then also $\exp(im\Omega t)u$ is also a solution, or, in other words, there is another phonon band with frequencies $\omega' = \omega + m\Omega$, with m a positive or negative integer. But there are also two phonon bands, with positive and negative frequencies, then, if there is a phonon (q, ω) , also there exists the phonon $(q, \Omega - \omega)$. As the unmodulated phonon band is $\in [\omega_0 = 1, \omega_{\max} = 1.01]$, for $\Omega \simeq 2$, a new phonon band appears $\in [\Omega - \omega_{\max} \simeq 0.98, \Omega - \omega_0 \simeq 1]$. The phonon bands in the modulated system change position, and $\Omega = 2\omega_b = 1.96$, but those bands are very close with the possibility of interfering, depending on the exact value of ω_b and actual modulated phonons. This problem does not exist for $\Omega \geq 3$ as the band $\Omega - \omega_{\text{phon}}$ is much separated.

For $\Omega = 2\omega_b$, and changing slightly ω_b , there is an interval where the two phonon bands coincide and then the system becomes stimulated by Ω and the variables diverge. A dissipation term can be added, but as this is a very special case, we prefer not to modify the system and simply avoid those combination of frequencies.

V.A. Period doubling $\Omega = 2\omega_b$

The subject of time-modulation is of recent interest in photonic topological insulators. For example, Floquet solitons, for which the intensity repeats after each driving period, were found experimentally in optical waveguide arrays with Kerr nonlinearity⁶ and period-doubled Floquet solitons were observed in a photonic topological insulator formed by an array of waveguides with a honeycomb pattern⁷. For these solutions, the intensity period is doubled. The same happens in a helically modulated honeycomb lattice as well and a sinusoidally driven SSH lattice. Period-doubled solitons also appear in²⁸. These references show that the period-doubling phenomenon

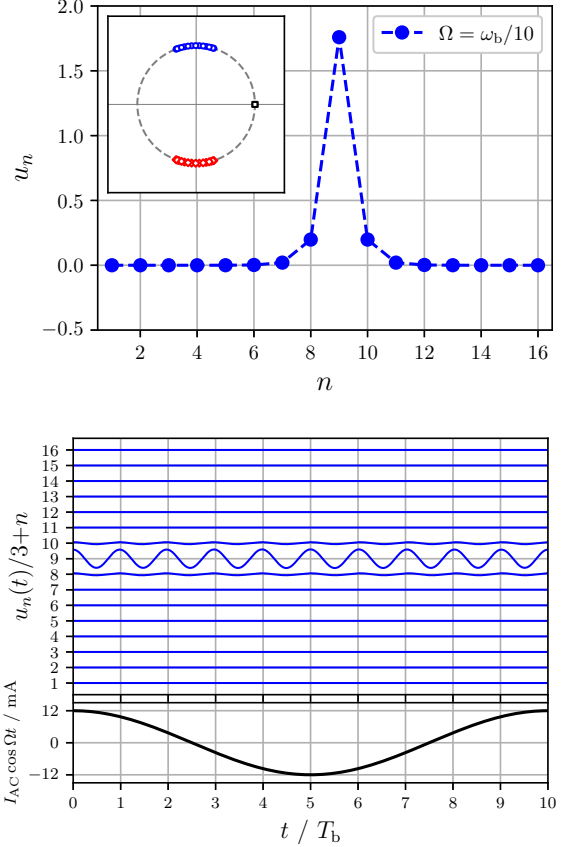


FIG. 8. (Top) Profile and Floquet eigenvalues for a breather with $\Omega = \omega_b/10$. The Krein signature of the Floquet eigenvalues is coded blue(+), red(-), black (zero). (Bottom) Evolution of the coordinates and the AC current. Parameters: $\kappa = 0.0052$, $\delta_1 = 0.1067$, $\delta_2 = 0.6996$, $\omega_b = 0.98$.

can appear in many different physical systems of interest and, in particular, photonic systems are ideal experimental devices to observe the connection between time modulation, topology and nonlinearity.

Period doubling also appears in our system. In figure 5-bottom we can see the evolution of the breather center and its neighboring sites, also the evolution of the energy, which is T_m -periodic and therefore also T_b -periodic. There is no net gain or loss of energy every period. The Floquet eigenvalues are also pictured in Fig. 6-top-left. The eigenvalues corresponding to the phonons form a pair of complex conjugate bands with frequencies $\omega_n = \omega_b + \theta_n/T_b$, as they have the same Krein signature²⁶ they form a structurally stable subset. There is also a close but separate eigenvalue with a localized eigenvector shown in Fig. 6-bottom, and thus corresponding to the breather solution. It has the opposite Krein signature of the phonons, meaning it can collide with the phonon with the closest frequency leaving the unit circle, which indicates that the breather is unstable and another solution exists, most likely an extended one, corresponding to

the merger of the breather with the upper phonon mode.

V.B. Cases $\omega_b = 3\Omega$ to $\omega_b = 10\Omega$

For $\omega_b = 3\Omega$, the breather is slightly unstable with two real multipliers very close to +1. In spite of that, simulations can be done to simulate the breather evolution with relatively long time. The Floquet multipliers are represented in Fig. 7 and the Fourier spectrum in a system with noise and $N = 160$ oscillators are shown.

For $\omega_b = n_T\Omega$, width $n_T = 1 \dots 10$, we have constructed breathers, for $n_T = 3, 4, 8$ breathers are unstable, while the rest are stable, therefore there is no apparent pattern. For example, for $n_T = 3$, there are two real eigenvalues slightly separated from +1, but, in spite of that, the breather has a long life.

VI. BREATHERS WITH $\Omega = \omega_b/n_T$

A peculiarity of this case is that the stability of the breather and the Floquet matrix have to be calculated for a time equal to the modulation period $T_m = n_T T_b$ as the coordinates, and velocities have to repeat, but also the forces which depend on time and only repeat after T_m . Therefore, the phonon band appear with Floquet exponents multiplied by n_T and spread out as they are given by $\theta_q = \omega_q T_m = n_T \omega_q T_b$ for a phonon of frequency ω_q .

In this section we separate the study of the Sievers-Takeno mode¹ or single breather, from the Page mode², or double breather. Values $n_T = 1, 2, \dots, 32$ are considered and a breather obtained. For $n_T = 32, \dots, 40$ phonobreathers²⁹ appear as explained in Sec. VI.B.

VI.A. Sievers-Takeno mode: single ILM with $\omega_b = n_T\Omega$

A stationary, single ILM or breather is a localized periodic vibration with a given frequency ω_b and with a single site, that we call the central one, having a large amplitude with respect to the phonons, and the amplitude of the neighbors diminishing rapidly with their distance to the center. They are often constructed from the anti-continuous limit with a single excited oscillator and the other at rest^{4,29,30}

In our system, the unmodulated system dispersion relation is given by $\omega^2 = \omega_0^2 + 2\kappa(1 - \cos(q))$, with a minimum frequency $\omega_0 = 1$. As the nonlinear part of the on-site potential is soft, because the dominant term is $o(3)$, stationary breathers or ILMs will have a frequency ω_b below the minimum frequency ω_0 . As demonstrated in Sec. IV, for a time-modulated system, the modulating frequency Ω , is commensurate with ω_b , and in this subsection, we consider the case $\Omega = \omega_b/n_T$. By using the shooting method, we tried and obtained exact ILMs for many values of n_T , as 1, 2, … 40. We present here only

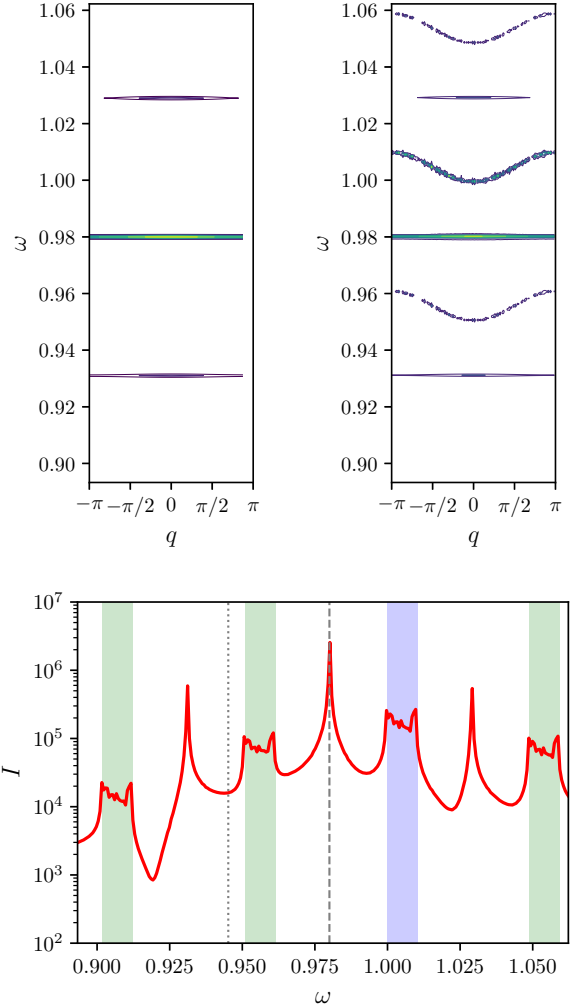


FIG. 9. Case $\Omega = \omega_b/20$. (Top) Frequency-momenta representation with scaled frequency. To the left for $N = 16$ sites, and to the right for $N = 160$ and noise added. See text. (Bottom) Spectra of the Fourier intensities in arbitrary units with respect to the scaled frequency. See text. Parameters: $\kappa = 0.0052$, $\delta_1 = 0.1067$, $\delta_2 = 0.6996$, $\omega_b = 0.98$.

some results with $\omega_b = 0.98$, that is, very close to the minimum frequency $\omega_0 = 1$ for the unmodulated system.

We construct the ILM in a small lattice with $N = 16$ cantilevers, and check its stability by constructing the monodromy matrix and obtaining the Floquet multipliers and exponents²⁶. Then, we embed the initial positions and within a larger lattice with $N = 160$ particles with some small random noise velocities, let it evolve and perform the XFFT to check the results. An example $\Omega = \omega_b/10$ with $\omega_b = 0.98$ can be seen in Fig. 8. The top panel shows the profile at $t = 0$ and the Floquet eigenvalues, showing its stability. The bottom panel illustrates the evolution of the variables for a period of the AC current.

We choose the case $\Omega = \omega_b/20$ with $\omega_b = 0.98$, to

illustrate the frequency-momenta representation as it is more easily seen. The top-right panel of Fig. 9-top-left shows the numerical XFFT (see App. B.1) of an exact breather at zero temperature in a small system with $N = 16$. The breather appears as a horizontal line corresponding to the breather frequency $\omega_b = 0.98$, with two other breather bands at frequencies $\omega_b \pm \Omega$. The lines are extended to almost all the momenta because the breather is extremely localized. No phonons appear.

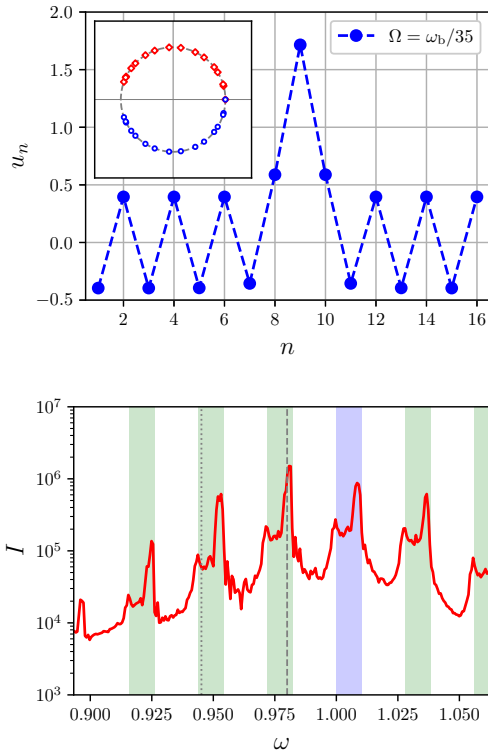


FIG. 10. (Top) For $\Omega < \omega_b/33$, a phonobreather, appears with a background wave to the ILM. The inset shows the Floquet eigenvalues with the Krein signature coded blue(+), red(-), black (zero). (Bottom) Fourier spectra. See text. Parameters: $\kappa = 0.0052$, $\delta_1 = 0.1067$, $\delta_2 = 0.6996$, $\omega_b = 0.98$.

Fig. 9-top-left shows the XFFT of the same breather but located within a larger system with $N = 160$ and thermalized with initial random velocities. The breather survives and the phonon band becomes apparent. Two replicas of the phonon band can be seen with frequencies $\omega = \pm\Omega + \sqrt{\omega_0^2 + 2\kappa(1 - \cos(q))}$, and also two replicas of the breather band with frequencies $\omega_b \pm \Omega$. Each breather line replica is located below the corresponding phonon band replica. Other replicas with weaker intensity are out of the frame.

Fig. 9-bottom shows the numerical spectra obtained for the larger lattice with noise, adding up the intensities for all the particles at the same time. We can also see that also that the frequencies $\omega_b \pm \Omega$ appear displaced $\omega_0 - \omega_b = 1 - 0.98 = 0.02$ above and below the bottom

of the secondary dispersion curves.

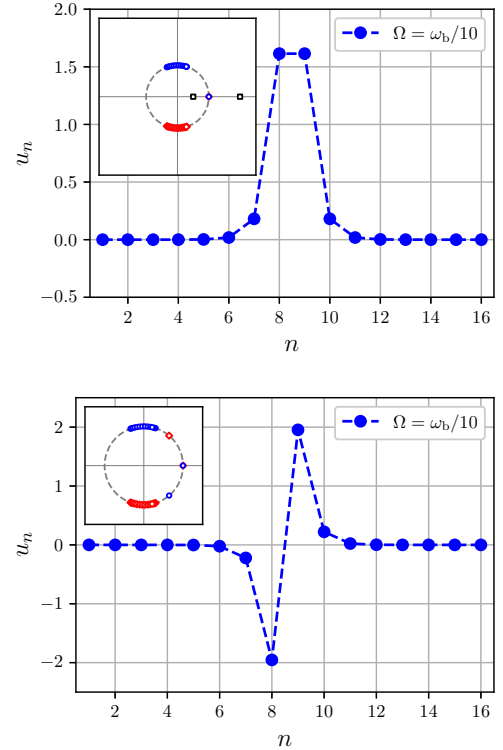


FIG. 11. (Top) For $\Omega < \omega_b/10$, profile of the unstable in-phase Page mode. (Bottom) The stable anti-phase Page mode with the same parameters and modulating frequency. The insets show the Floquet eigenvalues with the Krein signature coded blue(+), red(-), black (zero). Parameters: $\kappa = 0.0052$, $\delta_1 = 0.1067$, $\delta_2 = 0.6996$, $\omega_b = 0.98$.

VI.B. Phonobreathers: single ILM with phonon background for $\omega_b = n_T \Omega$

Although obtaining an ILM for increasing n_T is possible, as Ω becomes smaller, the upper secondary ILM band $\omega_b + \Omega$ collides with the upper frequency of the phonon band $\omega_{\max} = \sqrt{\omega_0 + 2\kappa(1 - \cos(\pi))} = \sqrt{\omega_0 + 4\kappa} = \omega_b + \Omega$, or $\Omega = \omega_{\max} - \omega_b$ and $\omega_b/\Omega \simeq 32.3$, for the values $\omega_0 = 1$ and $\kappa = 0.0052$. Then for $n_T > 30$ the upper phonons are excited and a extended wave with $q = \pi$ profile appears as the background of the ILM, with smaller but comparable amplitude, forming a *phonobreather*. A phonobreather is a periodic solution on a nonlinear system formed by a breather with a background of homogeneous amplitude. They were first described by Marín and Aubry^{5,29,31}. The background is not a phonon as it is not a solution of the linearized system and has a significant amplitude, it can also be described as a nonlinear extended wave.

The profile of the phonobreather can be seen in Fig. 10-

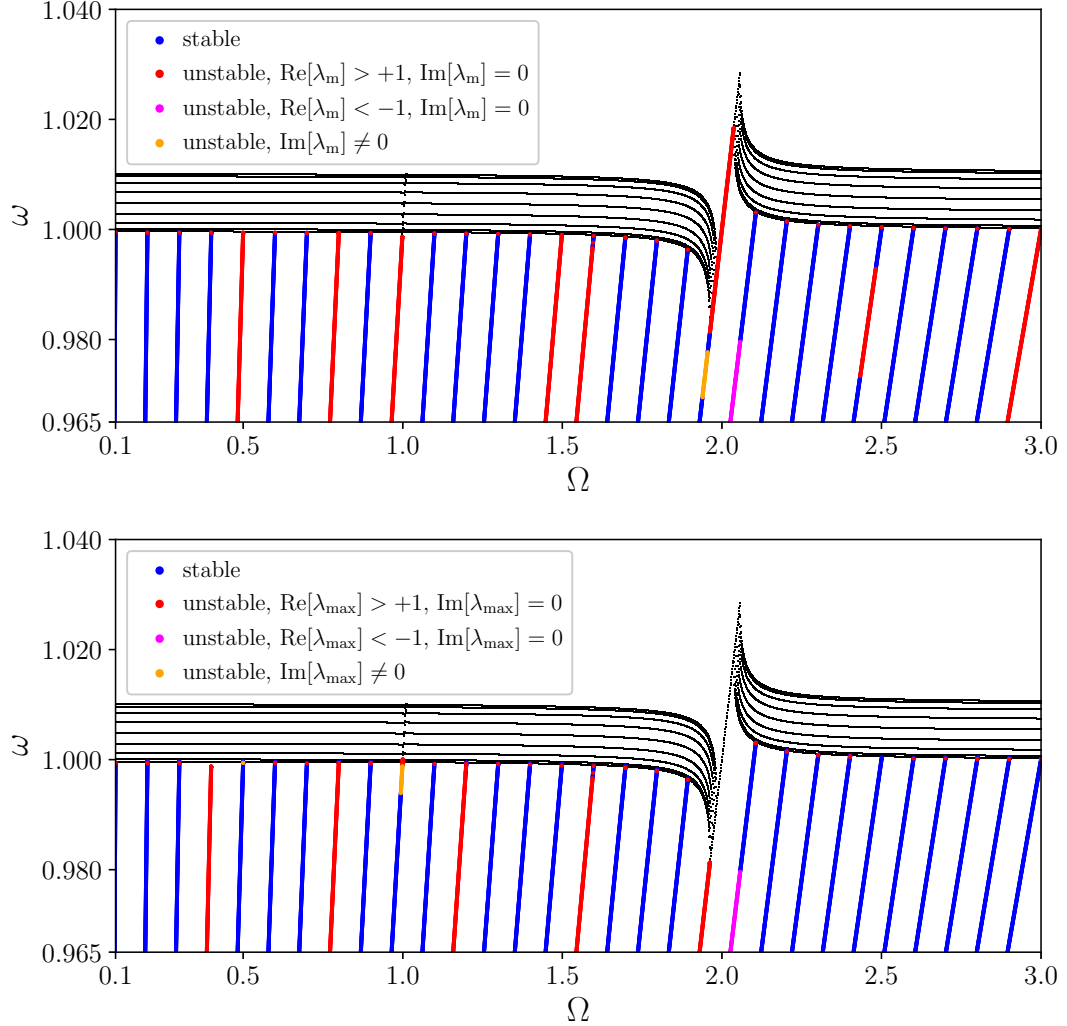


FIG. 12. (Top) ST in-phase breathers (Bottom) ST in-quadrature breathers. Evolution of the frequencies of phonons and breathers with indication of their stability. λ_{\max} denotes the eigenvalue with the maximum absolute value. The breather/modulation frequency ratios correspond to $\omega_b/\Omega = m_b/m_m$ for $m_b = 10$ and $m_m = [2, \dots, 30]$, that is, $\omega_b/\Omega = m_b/m_m = [5, 3.333, \dots, 1, \dots, 0.5, \dots, 0.3333]$. Particular cases of interest are Floquet breathers $\omega_b = \Omega$ and period-doubled breathers $\omega_b = \Omega/2$. See text for details. Parameters: $\kappa = 0.0052$, $\delta_1 = 0.1067$, $\delta_2 = 0.6996$.

(Top) and at the bottom of the same figure, the Fourier spectra, where the colliding of the top of the phonon bands can be seen merging with the ILM bands of upper order, while in Fig. 9-bottom they are well separated.

VI.C. Page modes with $\omega_b = n_T \Omega$

A Page mode^{2,4} is a double breather or ILM with two sites vibrating with the same amplitude, it can be bond-symmetric if both sites oscillate in-phase (iP), or bond-antisymmetric if they oscillate in anti-phase (aP). The iP mode is unstable and the aP is stable for an unmodulated Klein Gordon system with soft potential³². Both two modes appear also in the modulated system with the

same stability properties. Both mode profiles and Floquet multipliers are represented in Fig. 11 for $\omega_b = 10\Omega$. The XTFFT of the in-phase mode shows the appearance of another breather band closer to the bottom of the phonon band, which correspond to the unstable mode. Similar phenomena to the single ILM occur, i.e., formation of replicas of the phonon band and ILM band displaced $\pm\Omega$ in the frequency space and the excitation of the background forming a phonobreather when the secondary ILM band interacts with another replica of the phonon band just below.

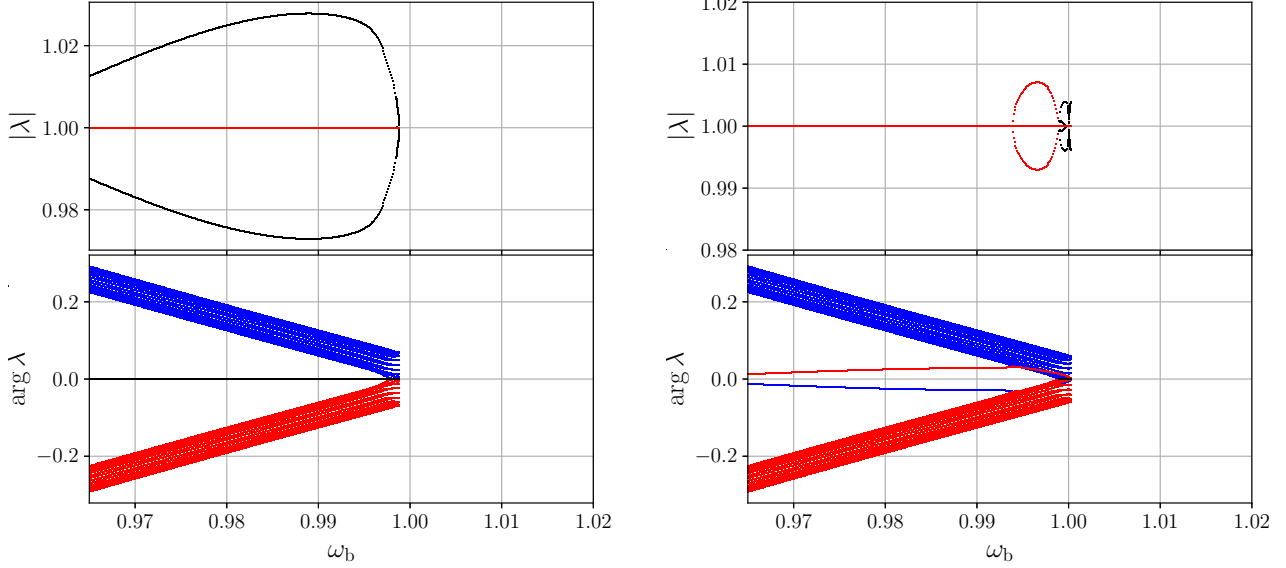


FIG. 13. Floquet breathers: $\omega_b = \Omega$: Evolution of the moduli and angle of the Floquet multipliers with the breather frequency. The sign of the Krein signature of the eigenvalue is represented by the code: blue +; red -; and black as zero. (Left) Breather in phase with the modulation; (Right) Breather in quadrature with the modulation. The in-phase breather (left) is unstable with the unstable eigenvalues in the positive real line. However, it can be continued until the two bands of phonon eigenvalues collide. The in-quadrature breather (right) is stable and structurally stable as the close eigenvalues have the same Krein signature and cannot abandon the unit circle. Eventually, the breather eigenvalue traverses the phonon bands with different Krein signatures bringing about oscillatory instabilities. It can be continued inside the phonon band. Parameters: $\kappa = 0.0052$, $\delta_1 = 0.1067$, $\delta_2 = 0.6996$, $N = 16$.

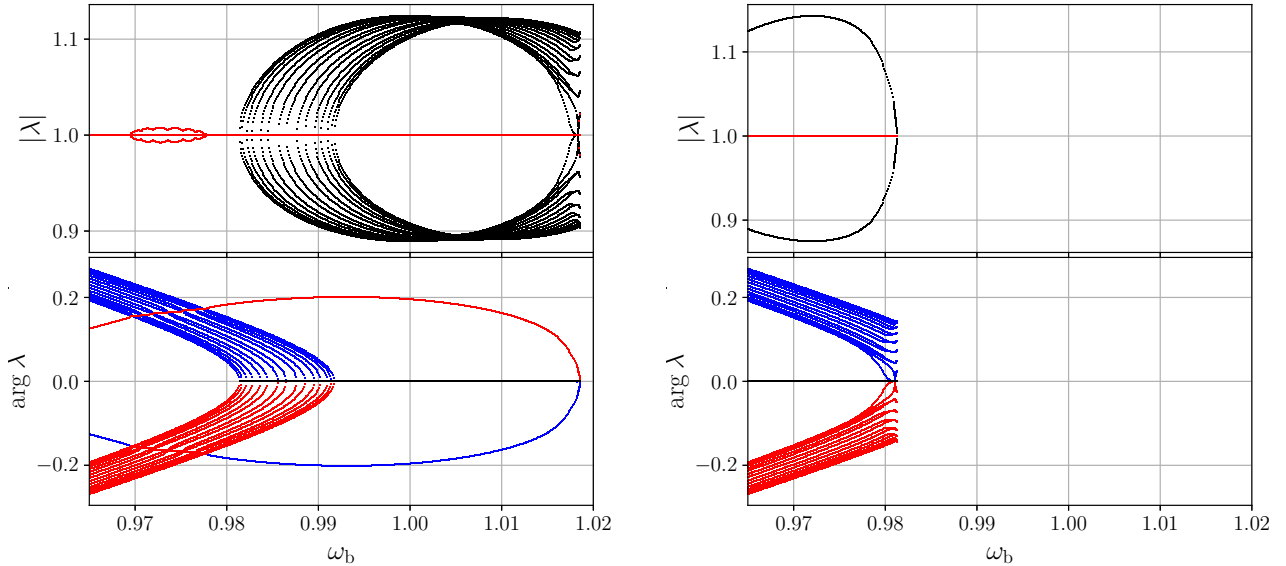


FIG. 14. Period-doubled breathers: $\omega_b = \Omega/2$: Evolution of the moduli and angle of the Floquet multipliers with the breather frequency. The sign of the Krein signature of the eigenvalue is represented by the code: blue +; red -; and black as zero. (Left) Breather in phase with the modulation; (Right) Breather in quadrature with the modulation. The in-phase breather (left) is stable and structurally stable until its eigenvalue traverses the phonon band where oscillatory instabilities occur, and becomes again stable after going out of the phonon band. The crossing is apparent as the phonons have actually a 2π extra angle. It can be continued briefly until the two phonon bands collide bring about instabilities at $+1$ as the system itself becomes unstable due to the resonance between the positive and negative phonon bands. In spite of that the breather can be continued. The in-quadrature period-doubled breather (right) is unstable for all frequencies, with unstable multipliers in the positive real line. Parameters: $\kappa = 0.0052$, $\delta_1 = 0.1067$, $\delta_2 = 0.6996$, $N = 16$.

VII. DEPENDENCE OF THE BREATHER STABILITY WITH THE FREQUENCY

In this section, we observe the changes of stability and instability when both the breather frequency ω_b and Ω change simultaneously as they are commensurate as deduced before in Sec. IV. The number of possible cases, i.e., depending of the fraction ω_b/Ω is huge, and the stability changes for each case are difficult to analyze. A panorama of the many cases is shown in Fig. 12, where a large number of cases for $\omega_b = (m_n/m_m)\Omega$, with $m_b = 10$ and $m_m = [2, \dots, 30]$ integers are presented indicating their stability or instability type. Note that those integers are not necessarily the same as in Lemma 1 and 2 in Sec. IV.A, but their ratio it is the same. The exact value of m_b and m_m requires finding the fundamental frequency of the breather, which it is not difficult, but it is not the object of this work.

Each breather calculation is represented by a circle with a color coding its instability as indicated by the legend. The breather circles make apparent lines with constant slope $\omega_b/\Omega = m_b/m_n$. A particularly interesting case is Floquet breathers with $\omega_b = \Omega$, where it can be seen that they can be continued into the phonon band. Other case of interest are period-doubled breathers, $\omega_b = \Omega/2$, for which there is a resonance with the negative phonon band $\omega_q^{(-)} = -\omega_q = -\sqrt{\omega_0^2 + 2\kappa(1 - \cos(q))}$, which is equivalent in a system with modulation frequency Ω to $\Omega - \omega_q$ and the two phonon band collide. As there is no dissipation the phonons take energy from the driving, grow and become nonlinear with their frequencies separating from the unmodulated phonon band.

When observing that a breather is unstable that may be due to interaction with phonons and other causes. A frequent one is that there is another breather with different structure which is stable for the same parameters. We tested for the existence and stability of breathers *in quadrature*, that is with a phase difference of 90° with the modulating term, with interesting results. Often, but by no means always, there is an interchange of stability between the in-phase breathers and the in-quadrature breathers as can be seen in Fig. 12.

In this section we concentrate into three cases of interest for ST breathers (i) Floquet breathers, with $\omega_b = \Omega$, period-doubled breathers $\omega_b = \Omega/2$, and period-halving breathers $\omega_b = 2\Omega$. All of them have been found experimentally in photonic systems^{6–8} and the comparison may be of interest.

In order present the stability evolution, a very useful method is the simultaneous representation of the moduli and arguments of the Floquet multipliers $|\lambda_i|$ and $\arg \lambda_i$. Usually, the breather appear as a pair of isolated eigenvalues and the phonons and a group or band of eigenvalues, and of course, this simple picture can change a lot. We think it is more practical to defer most of the explanation to the figure captions and give here some brief indications.

For Floquet breathers, the in-phase breather is unsta-

ble and the in-quadrature breather is stable, although the second one becomes unstable when its frequency collides with the phonon band as shown in Fig. 13.

For period-doubled breathers the opposite happens: the in-phase breather is stable becoming unstable when crossing the phonon band but becoming stable again until the system itself becomes unstable as the two phonon bands collide. The in-quadrature breather is unstable but can be continued until the collision of the phonon bands. This properties can be seen in Fig. 14.

For period-halved breathers, the in-quadrature breather is again stable and the in-phase ones are unstable. The plots in this cases are trivial and not represented.

VIII. CONCLUSIONS

We have modified a previous system corresponding to a physical model of cantilever arrays with on-site potential provide by electromagnets so as the on-site potential can be modulated both in time and space with DC and AC currents.

We have deduced their equations both in the linear and nonlinear range. We have obtained theoretically and observed numerically the change in the dispersion bands for space and time modulation separately and together. We have adapted the theory of exact breathers to time-modulated systems deducing that the modulation and breather frequencies in the moving frame should be commensurate as a necessary condition for breather existence.

We have analyzed the peculiarities of the stability analysis for time-modulated systems with the construction of and extended symplectic system.

First, breathers with a frequency multiple of the modulating one are studied and their properties analyzed.

For the modulating frequency smaller than the breather's one, we have found single breathers and double breathers, both symmetric and anti-symmetric. When the modulating frequency becomes small a phono-breather with extended background appears.

We have analyzed with detail the evolution of the stability or instability as the frequency changes for in-phase breathers and in-quadrature breathers, observing that for some cases they interchange their stability. We have paid particular attention to equal-period, doubled-period and halved-period Floquet breathers, that appear in photonic systems, observing the evolution of the Floquet eigenvalues with the frequency, obtaining insight of the phenomena.

Some theoretical results on moving breathers in modulated systems presented in this article will be numerically studied and checked in a forthcoming article.

This study reveals that this relatively simple system provides a huge variety of Floquet breathers which may also appears in other space-time modulated materials also known as dynamic metamaterials³³.

ACKNOWLEDGEMENTS

JFRA acknowledges the Laboratory of Microdynamics at the University of Osaka for hospitality.

All the authors would like to acknowledge Serge Aubry for the inspiration of his work. JFRA, in particular, although never worked directly with him, he did so with close collaborators as Robert Mackay and José Luis Marín in Cambridge, in 1997, where discussions with them over Aubry's publications became his introduction to research in this field.

FUNDING

JFRA and VJSM thanks grant PID2022-138321NB-C22 funded by MICIU/AEI/ 10.13039/501100011033 and ERDF/EU.

MK acknowledges support from JSPS Kakenhi (C) No. 24K07393 and 21K03935.

YD acknowledges support from JSPS Kakenhi (C) No. 24K14978.

Appendix A: Notation

To present formally the theory, we will use the ket and bra notation. The nice thing of that notation is that the properties of operations with vectors, change of basis, and operators appear as the simple juxtaposition of kets and bras. We present here this notation, more details can be read in Ref.¹⁹ and in Ref.³² applied to breather theory.

For our purposes, let us consider initially a ket $|\phi\rangle$ as a vector which can be expressed in different bases. There are two bases of interest in the domain of H_0 , the first one is given by $|n\rangle$'s, with $n = 0 : N - 1$, acting on any eigenfunction $|u\rangle$ of H_0 as $\langle n|u\rangle = u_n$. In that same basis is the column matrix $|n\rangle = [0, 0, \dots, 0, 1, 0, \dots, 0]'$, with the only 1 in position n and the rest zeros. A vector of positions are $|u\rangle = [u_1, u_2, \dots, u_n]'$ can be seen as $|u\rangle = \sum_{n=0}^{N-1} u_n |n\rangle$.

The bra $\langle\phi|$ is the Hermitian conjugate, so $\langle\phi|$ is a row matrix with elements the complex conjugates of the elements of $|\phi\rangle$. In this way, a bracket $\langle\phi_1|\phi_2\rangle$ is the scalar product $\sum_{n=0}^{N-1} \phi_{1,n}^* \phi_{2,n}$. Trivially $\langle n|n'\rangle = \delta_{n,n'}$. So the basis $\{|n\rangle\}$ is orthonormal. $\langle n|\phi\rangle = \phi_n$ as the scalar product by a unit basis vector and therefore the component of $|\phi\rangle$ in the direction of the unitary vector, or the component in that basis.

A dyad $|\phi_1\rangle\langle\phi_2|$ is a linear operator acting on kets as $|\phi_1\rangle\langle\phi_2||\phi_3\rangle = \langle\phi_2|\phi_3\rangle|\phi_1\rangle$

Any linear operator H can be expressed in a given basis as a sum of dyads as $H = \sum_{n=0}^{N-1} \sum_{n'=0}^{N-1} H_{n,n'} |n\rangle\langle n'|$, with $H_{n,n'} = \langle n|H|n'\rangle$ being the elements of the matrix representation of H in the basis $\{|n\rangle\}$.

The second basis is the momenta basis, and it is given in the $\{|k\rangle\}$ basis as:

$$|q_k\rangle = |k\rangle = \frac{1}{\sqrt{N}} \sum_{n=0}^{N-1} \exp(-i\frac{2\pi kn}{N}) |n\rangle, \quad \text{then}$$

$$|n\rangle = \frac{1}{\sqrt{N}} \sum_{k=0}^{N-1} \exp(i\frac{2\pi kn}{N}) |k\rangle. \quad (A1)$$

The second expression is the representation of $|n\rangle$ in the $|k\rangle$ -basis.

The following relations are useful and easy to obtain:

$$\langle n|n'\rangle = \delta_{n,n'} \quad ; \quad \langle k|k'\rangle = \delta_{k,k'} \quad ; \quad (A2)$$

$$\langle k|n\rangle = \frac{1}{\sqrt{N}} \exp(i\frac{2\pi kn}{N}) \quad ; \quad \langle n|k\rangle = \frac{1}{\sqrt{N}} \exp(-i\frac{2\pi nk}{N}) \quad (A3)$$

The identity operator is given by $I = \sum_{n=0}^{N-1} |n\rangle\langle n| = \sum_{k=0}^{N-1} |k\rangle\langle k|$, then

$$|u\rangle = \sum_{n=0}^{N-1} |n\rangle\langle n|u\rangle = \sum_{n=0}^{N-1} u_n |n\rangle, \quad \text{and}$$

$$|u\rangle = \sum_{k=0}^{N-1} |k\rangle\langle k|u\rangle = \sum_{k=0}^{N-1} F_k(u) |k\rangle, \quad (A4)$$

where $\langle n|u\rangle = u_n$, is the n -component of $|u\rangle$ in the $\{|n\rangle\}$ basis, and $\langle k|u\rangle = F_k(u)$ is the k -component of $|u\rangle$ in the $\{|q_k\rangle\}$ basis.

Using the appropriate form of the identity operator we can obtain the relationship between u_n and $F_k(u)$, that is the inverse and direct discrete Fourier transforms.

$$u_n = \langle n|u\rangle = \langle n| \left(\sum_{k=0}^{N-1} |k\rangle\langle k| \right) |u\rangle = \sum_{k=0}^{N-1} \langle n|k\rangle F_k(u)$$

$$= \sum_{k=0}^{N-1} \frac{1}{\sqrt{N}} \exp(-i\frac{2\pi nk}{N}) F_k(u), \quad (A5)$$

$$F_k(u) = \langle k|u\rangle = \langle k| \left(\sum_{n=0}^{N-1} |n\rangle\langle n| \right) |u\rangle$$

$$= \sum_{n=0}^{N-1} \langle k|n\rangle\langle n|u\rangle = \sum_{n=0}^{N-1} \frac{1}{\sqrt{N}} \exp(i\frac{2\pi nk}{N}) u_n \quad (A6)$$

A.1. Functions of position and time

Suppose we have a function $u =$ of the particle number n and time t , its value at a particle and time $u_n(t)$, are the components of the function u represented as the ket $|u\rangle$ in the basis with elements $|n, t\rangle$, i.e. $\langle n, t|u\rangle = u_n(t)$. In principle, t is a continuous variable but, in practice, it is a discrete one obtained by the sampling of numerical integration. So, if there are N_t time samples,

$t_l = l\Delta t$, with $l = 0 : N_t - 1$ and Δt the sampling interval. We change the basis notation to $|n, l\rangle$, with $\langle n, t|u\rangle = u_n(t_l) = u_n(l\Delta t)$ and

$$|u\rangle = \sum_{n=1}^N \sum_{l=0}^{N_t-1} u_n(t_l) |n, l\rangle.$$

The basis $|n, l\rangle$ is orthonormal, i.e. $\langle n, l|n', l'\rangle = \delta_{n,n';l,l'}$.

We assume that $u_n(t_l + N_t) = u_n(t_l)$, i.e., that u is time periodic with period $T_f = N_t\Delta t$. This is not a limitation as T_f is large enough that it has no consequences, similarly to Born-Von Karman boundary conditions in space.

Then, the alternative basis is given by the harmonic functions $|k, s\rangle$, with components:

$$\langle n, l|k, s\rangle = \frac{1}{\sqrt{NN_t}} \exp(-i[q_k n - \omega_s t_l]), \quad (\text{A7})$$

with period T_f , i.e., $\omega_s = \frac{2\pi s}{T_f} = \frac{2\pi s}{N_t \Delta t}$, ($s = 0 \dots N_t - 1$)

with maximum frequency $\frac{2\pi}{\Delta t}$. Usually, frequencies are shifted so as the zero frequency is the middle and then the maximum frequency is the Nyquist frequency $2\pi/2\Delta t$. Note that Δt determines the largest frequency, but the resolution is given by $\frac{2\pi}{T_f}$, that is, it depends on the final time.

The basis $|k, s\rangle$ is also orthonormal as

$$\langle k, s|k', s'\rangle = \delta_{k,k';s,s'}. \quad (\text{A8})$$

Therefore,

$$\langle k, s|u\rangle = \sum_{k=0}^{N-1} \sum_{s=0}^{N_t-1} \langle k, s|n, l\rangle \langle n, l|u\rangle \quad (\text{A9})$$

$$= \frac{1}{\sqrt{NN_t}} \sum_{k=0}^{N-1} \sum_{s=0}^{N_t-1} \exp(-i[q_k n - \omega_s t_l]) u_n(t_l) \quad (\text{A10})$$

We can also obtain the expression of $\frac{d^2}{dt^2}$ in k, s space. For that:

$$\frac{d^2}{dt^2} |k', s'\rangle = -\omega_{s'}^2 |k', s'\rangle \quad (\text{A11})$$

and then:

$$\langle k, s| \frac{d^2}{dt^2} |k', s'\rangle = -\omega_s^2 \delta_{k,k';s,s'} \quad (\text{A12})$$

Appendix B: Deduction of the effect of space-time modulation on the linear dispersion

In this section we consider the linear system described above in (7) which is valid for small displacements u_n .

For $\delta = 0$, the system is a well known, Klein-Gordon system, having a basis of solutions $\exp(iqn - \omega t)$, with $\omega_q^2 = \omega_0^2 + 4\kappa \sin^2(q/2)$. Note that for a given q there are two frequencies $\pm\omega$ that are also frequencies for $-q$.

For a finite system with N units and periodic boundary conditions the possible values of q are $q_m = 2\pi m/N$, with $m = 0, \dots, N-1$, this includes also negative values of the wavevector $q = -q'$, with $q' > 0$, as any wave number q is equivalent to $q \pm 2\pi n$. Also, any set of numbers $m' = m + n$, where n is any integer lead to an equivalent basis, a convenient one, centered around $q = 0$ is $-N/2, \dots, N/2 - 1$ if N is even or $-(N-1)/2, \dots, (N-1)/2$ if N is odd. An alternative basis in real space is given in $[-0.5, 0.5]$ by $\cos(qn - \omega t)$ and $\sin(qn - \omega t)$, but the exponential basis functions are 5000 , for example, when the system is supposed to be near or at thermal equilibrium and therefore all the linear modes or phonons are in principle excited. Then, we use the final positions and velocities, to run a simulation of similar length. Then, we use the results to perform the two dimensional fast fourier transform XFFT on the variable $u_n(t)$, that is,

$$F(q_k, \omega_r) = \frac{1}{\sqrt{N_t N}} \sum_{n=0}^{N-1} \sum_{l=0}^{N_t-1} \exp(i[q_k n - \omega_r t_l]) u_n(t_l),$$

with $t_l = \frac{l}{N_t} t_f$, $\omega_r = \frac{r}{N_t} \frac{2\pi}{\Delta t}$, for $l, r = 0 \dots N_t - 1$ and $q_k = \frac{k}{N} 2\pi$, for $k = 0 \dots N - 1$. The sampling interval $\Delta t = \frac{t_f}{N_t}$ is larger than the integration step to avoid very large matrices as the maximum frequency $2\pi/\Delta t$ does not need to be very large because the frequencies are of the order of ω_0 and Ω . On the other hand the frequency precision $\Delta\omega = \frac{2\pi}{N_t \Delta t} = \frac{2\pi}{t_f}$, is inversely proportional to t_f , therefore a large value of it is convenient, both to obtain precision for the frequency and for the results to be generic enough.

The intensities are defined as $I(\omega_i, q_n) = |F(\omega_i, q_n)|^2$, normalized to unity. To visualize the dispersion curves, we represent a number of lines in contour plots, typically ten, to get a clear picture. However, all the modes do not have the same probability to occur, the density of states may be small, and theoretically existing modes have small intensities and are difficult to discriminate from the noise background, those dispersion lines are *weak*. Presently, we do not have a means to calculate theoretically those intensities.

This method is changed to check that the results do not depend on the details, the random distribution can be applied only to momenta or to both coordinates and momenta; we can change the thermalization time, simulation time, sampling time interval, number of particles, etc. This method will also be used with a superposed breather in other sections.

The result of the simulation after thermalization are also used to obtain energy density plots. An example of both is shown in Fig. 2.

We can see that new dispersion bands appear roughly parallel to the unmodulated one and with their maxima and minima displaced.

B.2. Dispersion bands modification with only space modulation

In order to understand the result we will consider first the case $h = 2\pi/L$, where L is an integer, and $\Omega = 0$. In this case, the symmetry of the system $n \rightarrow n + 1$ is broken and substituted by the symmetry $n \rightarrow n + L$. Let us suppose that $\delta = 0$, but still the symmetry is broken, then, in order to be able to impose periodic boundary conditions, we need that $N = RL$ with R and integer number. Now, by Bloch theorem³⁴, the solutions are of the form $\exp(iqn)F(n, t)$, with $F(n, t)$ a solution with the periodicity of the lattice, whose period is now L , that is the elements of the basis are given by $u_{l,r} = \exp(iq_r n) \exp[i(q_r n - \omega_l t)]$. As the second factor has the periodicity of the new lattice $q_l = (2\pi/L)l$, with $l = 0, \dots, L-1$. If we impose periodic boundary conditions, then $u_{l,r}(n, t) = u_{l,r}(n + N, t)$, the second factor is automatically identical if $N = RL$ and the first factor becomes $q_r = 2\pi r/N$, with $r = 0, \dots, R-1$, as larger values of r can be written as $q'_r = 2\pi(r_1 R + r_2)/N = 2\pi(r_1 R + r_2)/LR = 2\pi r_1/L + 2\pi r_2/N$, and the first term is periodic in L and can be incorporated into $F(n, t)$. We can rewrite it as:

$$u_{n,t} = \exp(iqn) \exp(iq_r n) \exp(-i\omega_{l,r} t) \quad (B1)$$

$$= \exp(i\frac{2\pi r}{N}n) \exp(i\frac{2\pi l}{L}n) \exp(-i\omega_{l,r} t), \quad (B2)$$

with $r = 0, \dots, R-1$ and $l = 0 \dots L-1$. The original index $m = 0, \dots, N-1$ is given by $m = rL + l$, and the frequencies are given by

$$\omega_{l,r}^2 = \omega_0^2 + 2\kappa(1 - \cos(\frac{2\pi l}{L} + \frac{2\pi r}{N})). \quad (B3)$$

In the following, we use the standard notation of ket and bras summarized in Appendix A.

The solutions of the system $H_0|u\rangle = E_0|u\rangle$, with $E = \omega^2$ are given by the eigenvectors of H_0 with the same eigenvalue $E = \omega^2$. There are two eigenvectors with the same eigenvalue, corresponding to $|k\rangle$ and $| - k\rangle$, the latter being equivalent to $|N - k\rangle$ under periodic boundary conditions. Their eigenvalues are $E_0 = \omega^2 = \omega_0^2 + 2\kappa(1 - \cos(\frac{2\pi k}{N}))$.

The solution to the eigenvalue equation of the perturbed Hamiltonian

$$(H_0 + \delta H_1)|\phi\rangle = (E_0 + \delta E_1)|\phi\rangle$$

will be in the first approximation close to the eigenspace of E_0 , that is some linear combination of $|k_1\rangle \equiv |k\rangle$ and $|k_2\rangle \equiv | - k\rangle$ (it can be done with the cosine and sine solutions but the theory has to be reformulated and does not add any value). So, let us suppose that $|\phi_1\rangle$ is a linear combination of the orthogonal eigenvectors, i.e., $|\phi_1\rangle = \alpha|k_1\rangle + \beta|k_2\rangle$ and then, we obtain

$$E_0|\phi\rangle = H_0|\phi\rangle \quad \text{and} \quad E_1|\phi\rangle = H_1|\phi\rangle,$$

and we can write $|\phi\rangle = |\phi_1\rangle$. The first equation holds because ϕ is in the E_0 -eigenspace of H_0 . Substituting $|\phi_1\rangle$ and using that H_1 is linear, we obtain:

$$E_1(\alpha|k_1\rangle + \beta|k_2\rangle) = \alpha H_1|k_1\rangle + \beta H_1|k_2\rangle.$$

Multiplying by the left by $\langle k_1|$ and $\langle k_2|$ and using that $\langle k_1|k_2\rangle = \delta_{1,2}$, we obtain:

$$\alpha E_1 = \alpha \langle k_1|H_1|k_1\rangle + \beta \langle k_1|H_1|k_2\rangle \quad (B4)$$

$$\beta E_1 = \alpha \langle k_2|H_1|k_1\rangle + \beta \langle k_2|H_1|k_2\rangle \quad (B5)$$

In other words and in general, for any number of degenerate orthonormal eigenvectors $|k_i\rangle$ with the same eigenvalue, the corrections E_1 to the initial eigenvalue E_0 are given by the eigenvalues of the matrix M , which is the matrix representation of H_1 in the E_0 -subspace, or, explicitly

$$M_{ij} = \langle k_i|H_1|k_j\rangle \quad (B6)$$

The eigenvectors of M provide the linear combination of $|k_i\rangle$ with a eigenvalue E_1^i . By construction M is hermitian $M_{ij} = M_{ji}^*$ and the eigenvalues E_1^i are real.

What is left is to obtain M , which is done by

$$\begin{aligned} \langle k_i|H_1|k_j\rangle &= \langle k_i| \left(\sum_{n=0}^{N-1} |n\rangle\langle n| \right) H_1 \left(\sum_{n=0}^{N-1} |n'\rangle\langle n'| \right) |k_j\rangle \\ &= \sum_{n=0}^{N-1} \sum_{n'=0}^{N-1} \langle k_i|n\rangle\langle n|H_1|n'\rangle\langle n'|k_j\rangle \end{aligned} \quad (B7)$$

In our case $H_1|n\rangle = \cos(hn)|n\rangle$ and $\langle n|H_1|n'\rangle = \cos(hn)\delta_{n,n'}$. Therefore, we obtain:

$$\langle k_i|H_1|k_j\rangle = \frac{1}{N} \sum_{n=0}^{N-1} \exp(i\frac{2\pi k_i n}{N}) \cos(hn) \exp(-i\frac{2\pi k_j n}{N}) \quad (B8)$$

If $h = 2\pi m$, with m integer, then $\langle k_i | H_1 | k_i \rangle = 1$, but it is a case of no interest, as the system would have again unit lattice distance (or less). Otherwise, if $h \neq 2\pi m$:

$$\langle k_i | H_1 | k_i \rangle = \frac{1}{N} \sum_{n=0}^{N-1} \cos(hn). \quad (\text{B9})$$

As it does not depend on k_i , the diagonal terms of M are equal and real, given by:

$$a = M(1, 1) = M(2, 2) = \Re \left(\frac{1}{N} \sum_{n=0}^{N-1} \exp(ihn) \right). \quad (\text{B10})$$

Let us call $b = M(1, 2) = M(2, 1)^*$, then, the eigenvalues of M are $E_1 = \Delta\omega^2 = a \pm |b|$. The value a represents a global shift of the dispersion curve, while b represents the separation in two values of ω^2 .

However, the term (B10) is bounded by 1 at $h = 0$, which is of no interest. It is also zero for $h = 2\pi/L$ with $L = N/R$, L and R integers. For other values of $h > 0$ it is very small except at the proximity of $h = 0$. Therefore, the global shift provided by the modulation is very small.

The non-diagonal elements of M are complex conjugates and given by:

$$\begin{aligned} b &= \langle k | H_1 | -k \rangle = \frac{1}{N} \sum_{n=0}^{N-1} \exp(i2q_k n) \cos(hn) \\ &= \frac{1}{2N} \sum_{n=0}^{N-1} \exp(i[2q_k + h]n) + \frac{1}{2N} \sum_{n=0}^{N-1} \exp(i[2q_k - h]n). \end{aligned} \quad (\text{B11})$$

This expression is bounded by 1, taking its maximum absolute value 1 when both $2q_k$ and h are integer multiples of 2π . But that case is of no interest as it implies $L = 1$ with no symmetry breaking, so $h \leq \pi$. However, b is close to 0.5 if at least one of the two sums in (B11) is N , which happens for either $2q_k + h = 2\pi m$ or $2q_k - h = 2\pi m'$, for m and m' integers. This condition is fulfilled for $q_k \in [0, 2\pi]$ at four values, although they degenerate to a single value when $h = \pi$ as $-h/2 = h/2 - \pi$.

Therefore if $h < \pi$:

$$\begin{aligned} b &= M(1, 2) = \langle k | H_1 | -k \rangle \simeq 0.5 \quad \text{for} \\ q &= \frac{h}{2}, q = \frac{h}{2} + \pi, q = 2\pi - \frac{h}{2}, q = \pi - \frac{h}{2}. \end{aligned} \quad (\text{B12})$$

Therefore, the effect of the modulations is a small shift in $\omega^2(q)$ of order δa and the degeneracy raising of the bands for the four given specific wavenumbers is of order $\delta/2$.

As an example, if $h = 2\pi/3$, then $a = 0$, and the values of q for which the bands split are $\pi/3, 2\pi/3, 4\pi/3, 5\pi/3$. Figure 15 shows the numerically obtained dispersion function and the theoretical results on degeneracy raising.

Note that the dispersion curves are represented

within the Brillouin zone before modulation $[0, 2\pi]$. The Brillouin zone after modulation is $[0, 2\pi/L] = [0, 2\pi/3]$, with $L = 3$ the new lattice distance after the breaking of the symmetry invariance. Phonon wavevectors $q > 2\pi/3$ have to be translated to $q - n2\pi/3$, with $n=1$ or 2 , to the new Brillouin zone. We think that this extended representation is clearer for the present context.

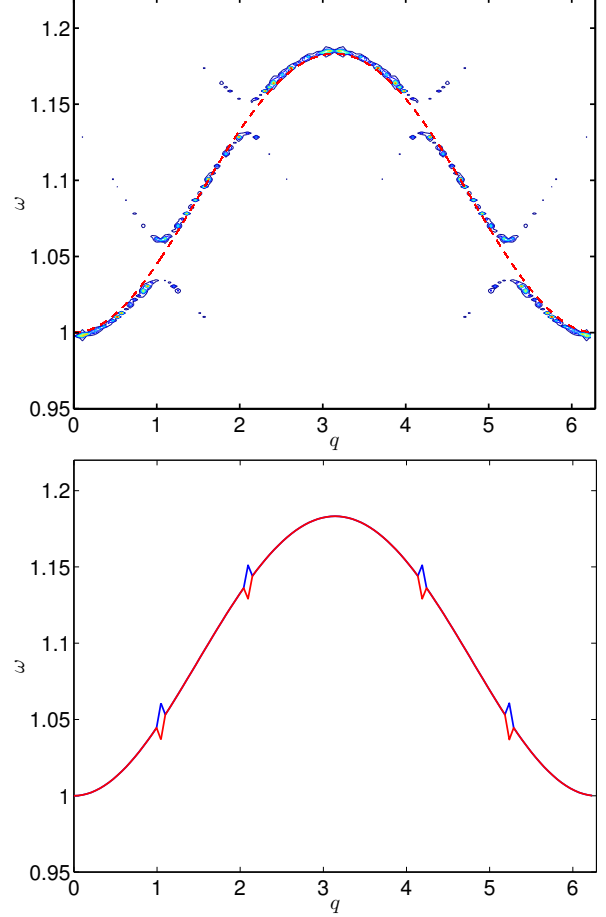


FIG. 15. **(Top:)** Numerical dispersion bands for $h = 2\pi/3$; **(Bottom:)** Theoretical degeneracy raising of the dispersion bands due to space modulation. Note that the Brillouin zone is $[0, 2\pi/3]$. See the text for explanation. Parameters: $\kappa = 0.10.055794$, $\delta = 0.05$, $\Omega = 0$.

B.3. Effect of only time modulation on the phonon bands

When $h = 0$, the effect of time modulation is to split the phonon band in several parallel bands separated by a frequency of Ω . They are obtained numerically as explained in App. B.1. Some bands are *weak*, meaning that their intensity in the XTFFT is small, presumably because their density of states is small. Some becomes so weak that they can not be seen into the background noise. The number of bands diminishes with increased frequency and eventually the bands disappear or are not

visible. Extra bands appear for frequency below $\omega_0 = 1$ although they are very weak when approaching $\Omega = \omega_0$. Frequencies multiples of ω_0 lead to a divergence of the system. Frequencies inside the phonon band excites the modes with that frequency.

These bands can be obtained analytically using the breakup of the time-invariance brought about by the time modulation. For that, we will use the notation and theory treated in Appendix A, taking into account the changes brought about by the time dependence of the on-site potential.

Consider the unmodulated version of Eq. (7)

$$\ddot{u}_n = -\omega_0^2 u_n + \kappa(u_{n+1} + u_{n-1} - 2u_n). \quad (\text{B13})$$

It is invariant under translations in time $t \rightarrow t + \Delta t$, where Δt is the sampling interval, which could be arbitrary, in principle. Let us choose $\Delta t = T_m/M$, with M an integer, that is $\Omega = 2\pi/T_m = M2\pi/\Delta t$. The addition of the term $-\delta \cos(\Omega t)u_n$ to the rhs of (B13) breaks this invariance. The modulated system is invariant only under larger translation of time $T_m = M\Delta t$, multiples of Δt . There is a breaking of the symmetry: the system is no longer invariant under the time shifts $t \rightarrow t + \Delta t$ but only under a subgroup of time shifts $t \rightarrow t + T_m = t + M\Delta t$.

The new solution is given by Bloch theorem^{35,36}, as $\exp(-i\omega t)$, multiplied by a periodic function with the period of the operator, that is

$$u = \exp(i[qn - \omega t]) \sum_{m=-M/2}^{M/2} A_m \exp(-im\Omega t),$$

with the coefficients A_m depending on q .

Then, the substitution of u into the dynamical system leads to (substituting $\cos(\Omega t) = (\exp(i\Omega t) + \exp(-i\Omega t))/2$):

$$(\omega + m\Omega)^2 A_m = [\omega_0^2 + 2\kappa(1 - \cos(q))] A_m + \frac{\delta}{2}(A_{m+1} + A_{m-1}), \quad (\text{B14})$$

or

$$(\omega + m\Omega)^2 A_m = \bar{\omega}_q^2 A_m + \frac{\delta}{2}(A_{m+1} + A_{m-1}), \quad (\text{B15})$$

where $\bar{\omega}_q$ is the unperturbed frequency for the wavenumber q . This is a complicated equation, but if δ is small with respect to Ω , we can suppress that term in the first approximation, that is

$$(\omega + m\Omega)^2 A_m = \bar{\omega}_q^2 A_m. \quad (\text{B16})$$

This equation has a solution corresponding to make all $A_k = 0$, except A_m , for each m , indicating that each solution is characterized by a harmonic of higher order of the modulating wave.

Then, we obtain:

$$\omega_{q,m} = -m\Omega + \sqrt{\bar{\omega}_q^2} = -m\Omega + \sqrt{\omega_0^2 + 2\kappa(1 - \cos(q))}. \quad (\text{B17})$$

Therefore, the main effect of the symmetry breaking is the appearance of bands separated by the frequency Ω almost parallel to the unperturbed dispersion band (UDB). However, the intensity of those bands tend to be smaller the further apart from the UDB. It is necessary to plot contours of small intensity in order to observe them.

Solving (B16), it is also possible to obtain $\omega = m\Omega - \bar{\omega}_q^2$, but this equation lead to a change of sign of the frequencies, corresponding to waves traveling in opposite direction, which are already obtained for negative wavenumbers q .

Two examples can be seen in Fig. 3

B.4. Dispersion bands for space-time modulation

Considering the system (7):

$$\ddot{u}_n = -\omega_0^2 u_n - \delta \cos(hn - \Omega t) u_n + \kappa(u_{n+1} + u_{n-1} - 2u_n). \quad (\text{B18})$$

The system is now 2π periodic in the variable $hn - \Omega t$, and the solutions can be written as the product of a plane wave multiplied by a function with the periodicity of the system. That is:

$$u = \exp(i[qn - \omega t]) \sum_{m=-M/2}^{M/2} A_m \exp(im[hn - \Omega t]).$$

Then, the substitution of u in the Hamiltonian leads to (substituting $\cos(hn - \Omega t) = (\exp(i[hn - \Omega t]) + \exp(-i[hn - \Omega t]))/2$):

$$(\omega + m\Omega)^2 A_m = [\omega_0^2 + 2\kappa(1 - \cos(q + mh))] A_m + \frac{\delta}{2}(A_{m+1} + A_{m-1}). \quad (\text{B19})$$

Assuming that δ is small with respect to Ω , we can obtain the independent solutions where all the $A_k = 0$, except one A_m each time, so it corresponds to a single harmonic with ω :

$$\omega = -m\Omega + \sqrt{\omega_0^2 + 2\kappa(1 - \cos(q + mh))} \quad (\text{B20})$$

An example can be seen in Fig. 4.

¹A. J. Sievers and S. Takeno, “Intrinsic localized modes in anharmonic crystals,” *Phys. Rev. Lett.* **61**, 970–973 (1988).

²J. B. Page, “Asymptotic solutions for localized vibrational modes in strongly anharmonic periodic systems,” *Phys. Rev. B* **41**, 7835–7838 (1990).

³S. Flach and A. V. Gorbach, “Discrete breathers in Fermi-Pasta-Ulam lattices,” *Chaos* **15**, 015112 (2005).

⁴S. Flach and A. V. Gorbach, “Discrete breathers. Advances in theory and applications,” *Phys. Rep.* **467**, 1–116 (2008).

⁵Serge Aubry, “Breathers in nonlinear lattices: Existence, linear stability and quantization,” *Physica D* **103**, 201–250 (1997).

⁶Sebabrata Mukherjee and Mikael C. Rechtsman, “Observation of Floquet solitons in a topological bandgap,” *Science* **368**, 856–859 (2020).

⁷Sebabrata Mukherjee and Mikael C. Rechtsman, “Period-doubled Floquet solitons,” *Optica* **10**, 1310–1315 (2023).

⁸Qianqian Kang, Zhaoyuan Wang, Xiaoqin Huang, Fengyi Cao, Jiaxin Li, Yi Hu, and Jingjun Xu, “Period-halving effect in Floquet photonic structures,” *Laser Photonics Rev.* , e02551 (2025).

⁹Ross Parker, Alejandro Aceves, Jesús Cuevas-Maraver, and P. G. Kevrekidis, “Floquet solitons in square lattices: Existence, stability, and dynamics,” *Phys. Rev. E* **105**, 044211 (2022).

¹⁰Magnus Johansson, Goran Gligorić, Aleksandra Maluckov, Petra P. Belićev, Rodrigo A. Vicencio, and Milutin Stepić, “Floquet lattice solitons in zigzag modulated waveguide arrays with zero average modulation: Exponential localization and linear stability,” *Chaos* **35**, 123107 (2025).

¹¹M. Sato, B. E. Hubbard, and A. J. Sievers, “Colloquium: Nonlinear energy localization and its manipulation in micromechanical oscillator arrays,” *Rev. Mod. Phys.* **78**, 137–157 (2006).

¹²Masayuki Kimura and Takashi Hikihara, “Coupled cantilever array with tunable on-site nonlinearity and observation of localized oscillations,” *Phys. Lett. A* **373**, 1257–1260 (2009).

¹³M. Sato and A. J. Sievers, “Driven localized excitations in the acoustic spectrum of small nonlinear macroscopic and microscopic lattices,” *Phys. Rev. Lett.* **98**, 214101 (2007).

¹⁴Masayuki Kimura and Takashi Hikihara, “Capture and release of traveling intrinsic localized mode in coupled cantilever array,” *Chaos* **19**, 013138 (2009).

¹⁵Masayuki Kimura, Yasuo Matsushita, and Takashi Hikihara, “Parametric resonance of intrinsic localized modes in coupled cantilever arrays,” *Phys. Lett. A* **380**, 2823–2827 (2016).

¹⁶Christopher Chong, Andre Foehr, Efstathios G. Charalampidis, Panayotis G. Kevrekidis, and Chiara Daraio, “Breathers and other time-periodic solutions in an array of cantilevers decorated with magnets,” *Math. Eng.* **1**, 489–507 (2019).

¹⁷Hirotaka Araki and Takashi Hikihara, “Shift manipulation of intrinsic localized mode in AC driven Klein Gordon lattice,” *Phys. Lett. A* **493**, 129270 (2024).

¹⁸Christopher Chong, Brian Kim, Evelyn Wallace, and Chiara Daraio, “Modulation instability and wavenumber bandgap breathers in a time layered phononic lattice,” *Phys. Rev. Res.* **6**, 023045 (2024).

¹⁹David J. Griffiths, *Introduction to Electrodynamics*, 5th ed. (Cambridge University Press, Cambridge, 2024).

²⁰Ding Chen, S. Aubry, and G. P. Tsironis, “Breather mobility in discrete φ^4 nonlinear lattices,” *Phys. Rev. Lett.* **77**, 4776–4779 (1996).

²¹Serge Aubry and Thierry Cretegny, “Mobility and reactivity of discrete breathers,” *Physica D* **119**, 34–46 (1998).

²²Sergej Flach and Konstantin Kladko, “Moving discrete breathers?” *Physica D* **127**, 61–72 (1999).

²³Juan F. R. Archilla, Yusuke Doi, and Masayuki Kimura, “Pterobreathers in a model for a layered crystal with realistic potentials: Exact moving breathers in a moving frame,” *Phys. Rev. E* **100**, 022206 (2019).

²⁴G. James and Y. Sire, “Travelling breathers with exponentially small tails in a chain of nonlinear oscillators,” *Commun. Math. Phys.* **257**, 51–85 (2005).

²⁵J. Gómez-Gardeñes, F. Falo, and L. M. Floría, “Mobile localization in nonlinear Schrödinger lattices,” *Phys. Lett. A* **332**, 213–219 (2004).

²⁶S. Aubry, “Discrete breathers: Localization and transfer of energy in discrete Hamiltonian nonlinear systems,” *Physica D* **216**, 1–30 (2006).

²⁷H. Marthinsen and B. Owren, “Geometric integration of non-autonomous linear hamiltonian problems,” *Adv. Comput. Math.* **42**, 313–332 (2016).

²⁸Yiming Pan and Bing Wang, “Time-crystalline phases and period-doubling oscillations in one-dimensional Floquet topological insulators,” *Phys. Rev. Res.* **2**, 043239 (2020).

²⁹J. L. Marín and S. Aubry, “Breathers in nonlinear lattices: Numerical calculation from the anticontinuous limit,” *Nonlinearity* **9**, 1501 (1996).

³⁰R. S. MacKay and S. Aubry, “Proof of existence of breathers for time-reversible or Hamiltonian networks of weakly coupled oscillators,” *Nonlinearity* **7**, 1623 (1994).

³¹J. L. Marín and S. Aubry, “Finite size effects on instabilities of discrete breathers,” *Physica D* **119**, 163–174 (1998).

³²J. F. R. Archilla, J. Cuevas, B. Sánchez-Rey, and A. Alvarez, “Demonstration of the stability or instability of multibreathers at low coupling,” *Physica D* **180**, 235–255 (2003).

³³Lingling Wu, Yong Wang, Kuochih Chuang, Fugen Wu, Qianxuan Wang, Weiqi Lin, and Hanqing Jiang, “A brief review of dynamic mechanical metamaterials for mechanical energy manipulation,” *Mater. Today* **44**, 168–193 (2021).

³⁴David J. Griffiths and Darrell F. Schroeter, *Introduction to Quantum Mechanics*, 3rd ed. (Cambridge University Press, Cambridge, 2018).

³⁵Josh C. Slater, “Interaction of waves in crystals,” *Rev. Mod. Phys.* **30**, 197–222 (1958).

³⁶E S Casseddy and A A Oliner, “Dispersion relations in time-space periodic media: Part i-Stable interactions,” *P. IEEE* **51**, 1342–1359 (1963).